MINI-VOLUME: SOLAR RADIOPHYSICS — RECENT RESULTS ON OBSERVATIONS AND THEORIES: INVITED REVIEWS

A review of solar type III radio bursts

To cite this article: Reid Hamish Andrew Sinclair and Ratcliffe Heather 2014 *Res. Astron. Astrophys.* **14** 773

View the article online for updates and enhancements.

INVITED REVIEWS

A review of solar type III radio bursts

Hamish Andrew Sinclair Reid[1] and Heather Ratcliffe[2]

[1] SUPA School of Physics & Astronomy, University of Glasgow, G12 8QQ, United Kingdom; *hamish.reid@glasgow.ac.uk*
[2] Centre for Space, Fusion and Astrophysics, Department of Physics, University of Warwick, CV4 7AL, United Kingdom

Abstract Solar type III radio bursts are an important diagnostic tool in the understanding of solar accelerated electron beams. They are a signature of propagating beams of nonthermal electrons in the solar atmosphere and the solar system. Consequently, they provide information on electron acceleration and transport, and the conditions of the background ambient plasma they travel through. We review the observational properties of type III bursts with an emphasis on recent results and how each property can help identify attributes of electron beams and the ambient background plasma. We also review some of the theoretical aspects of type III radio bursts and cover a number of numerical efforts that simulate electron beam transport through the solar corona and the heliosphere.

Key words: Sun: flares — Sun: radio radiation — Sun: X-rays, gamma rays — Sun: particle emission

1 INTRODUCTION

The Sun is the most efficient and prolific particle accelerator in our solar system. Electrons are regularly accelerated to near-relativistic energies by the unstable magnetic field of the solar atmosphere. Solar flares are the most violent example of such acceleration, with vast amounts of energy released when the solar magnetic field reconfigures to a lower energy state, releasing energy on the order of 10^{32} erg and accelerating up to 10^{36} electrons per second in the solar atmosphere (e.g. Emslie et al. 2012).

Solar radio bursts come in a variety of forms, classified by how their frequency changes in time, known as their frequency drift rate. Initially, three types of radio emission were named type I, II and III in order of ascending drift frequency (Wild & McCready 1950), with types IV and V introduced later. Each type has subtypes that further describe the array of complex behavior these radio bursts display. In this study we are going to concentrate on the most prolific type of solar radio burst, the type III radio burst. These are a common signature of near-relativistic electrons streaming through the background plasma of the solar corona and interplanetary space, offering a means to remotely trace these electrons. Moreover, their dependence on the local plasma conditions means they act as a probe of the solar coronal plasma and the plasma of the solar wind. The example type III burst
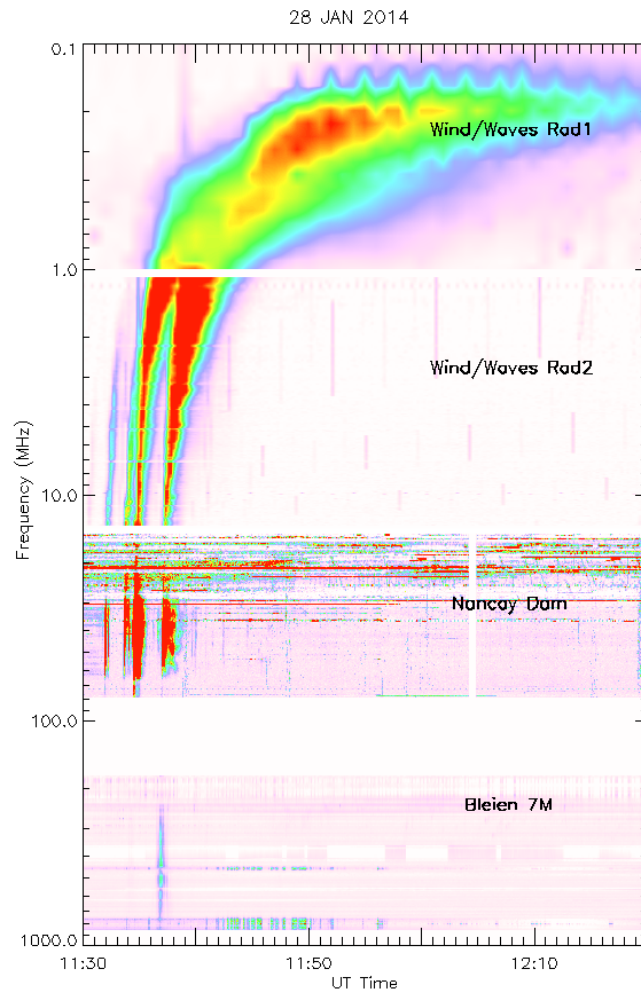
Fig. 1 An example of a dynamic spectrum from an interplanetary type III radio burst observed on the 28th January 2014. The 900–200 MHz frequencies are observed by the Bleien telescope (Benz et al. 2009a). The 80 to 15 MHz frequencies are observed by the Nancay (with the cedilla) Decametric Array (Lecacheux 2000). The 14 to 0.1 MHz frequencies are observed by the WAVES experiment onboard the WIND spacecraft (Bougeret et al. 1995). You can see a number of different type III bursts starting at different frequencies from < 100 MHz at 11:32 UT to > 1 GHz at 11:37 UT. All the radio bursts merge into one at the lowest frequencies of < 1 MHz.

in Figure 1 shows their main features; they are very bright, transient bursts that usually drift from higher to lower frequencies over time.

The precise mechanism for the acceleration of solar electrons is still debated but it is generally attributed to the reconfiguration of an unstable coronal magnetic field, resulting in the conversion of free magnetic energy to kinetic energy. This acceleration usually occurs at solar active regions but can occur when the magnetic field in a coronal hole interacts with the surrounding magnetic field (a process known as interchange reconnection). Moreover, type III radio bursts are observed in relation with X-ray bright points (Kundu et al. 1994).
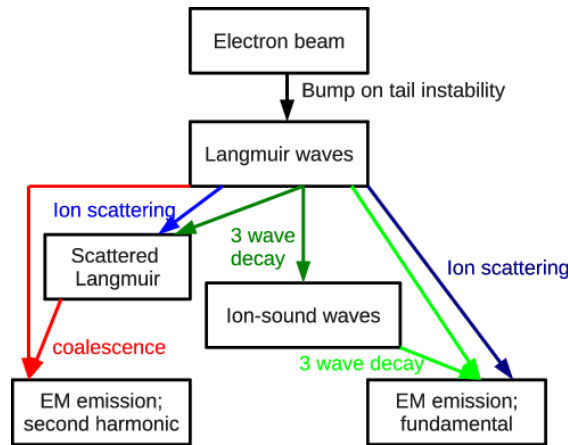
Fig. 2 A flow diagram indicating the stages in plasma emission in an updated version on the original theory (adapted from Melrose 2009).

The first theory of type III bursts was described by Ginzburg & Zhelezniakov (1958). They considered the two-stream instability of an electron beam which generates Langmuir (plasma) waves at the local plasma frequency that can be converted into electromagnetic emission. They proposed that scattering by plasma ions would produce radiation at the plasma frequency (the fundamental component), while the coalescence of two Langmuir waves could produce the second harmonic. The theory has been subsequently discussed and refined by many authors (e.g. Sturrock 1964; Zheleznyakov & Zaitsev 1970; Smith 1970; Smith et al. 1976; Melrose 1980c; Goldman 1983; Dulk 1985; Melrose 1987), but the basic two-step process, production of Langmuir waves followed by their conversion into EM emission, remains the same. An overview of the dominant processes is shown in Figure 2.

This *plasma emission mechanism* is now the generally accepted model for type III burst generation. Analytical calculations over many years have shown it is certainly capable of explaining the drift, brightness and harmonic structure of bursts. Alternatives, such as strong turbulence effects like Langmuir wave collapse (e.g. Goldman 1983), conversion of Langmuir waves directly into EM waves (e.g. Huang 1998) and emission via the maser mechanism (e.g. Wu et al. 2002), can explain some of the properties of type IIIs. Where relevant, we assume plasma emission throughout this review.

The purpose of this study is to give an overview on the type III radio burst as a probe of both accelerated electrons and the background plasma it travels through. In Section 2 we give a detailed account of the observational characteristics of type III radio bursts and we describe how they relate to the properties of the generating electron beam. Section 3 reviews in-situ plasma observations connected with type III bursts. In Section 4 we will cover some of the theoretical work that has been done on electron beams responsible for type III radio bursts. In Section 5 we will give an overview of the theory involved with the generation of electromagnetic emission from plasma waves. Finally we look towards the future in Section 6 by covering the "state of the art" simulation codes and the next generation of radio telescopes.

2 OBSERVED PROPERTIES OF TYPE IIIS

A solar type III radio burst is a transient burst of radio emission that starts at higher frequencies and drifts to lower frequencies as a function of time. Their durations, frequency extent and even how fast

they drift varies from burst to burst. Their size and intensity are different at different frequencies. The nonlinear emission mechanism can lead to substructure in the dynamic spectra like clumpy emission and harmonic pairs. There are a number of variants of type III bursts: some have positive drift rates in frequency, some have different polarization and some vary dramatically in frequency and time. Other wavelengths of light can also be observed at the same time as type III bursts.

We review the main properties of the radio emission that we call a type III burst. When relevant we also highlight what information can be deduced from the observations regarding both the exciting electron beam and the background heliospheric plasma. Type III radio bursts have been studied intensely for the last 60 yr so it is beyond our scope to mention all works that have been done on the subject. We try to focus on the most recent works and to mention the range and variability of each property.

2.1 Frequency and Time

2.1.1 Frequency extent

The starting frequency of type III bursts varies dramatically from burst to burst. During large solar flares type III bursts can start at frequencies in the GHz (e.g. Benz et al. 1983b; Staehli & Benz 1987; Benz et al. 1992; Meléndez et al. 1999). Typically type III bursts will start at 10s or 100s of MHz and can start at even lower frequencies. When two components are observed (see Sect. 2.3.2), the fundamental often starts at lower frequencies than the harmonic, with the ratio of their onset frequencies often as large as 1:3 or 1:5 (Suzuki & Sheridan 1978). When type III bursts are observed at high frequencies they are usually in groups corresponding to multiple accelerated electron beams during solar flares. The variation in starting frequency can be attributed to several causes. Bursts at very high frequency (GHz range) are subject to absorption and have to be intense to be visible above the quiet-Sun background. Moreover, collisions in the background plasma damp both electrons and plasma waves making it harder to generate radio emission (see Sect. 4.4). Favorable conditions for high frequency type III emission are acceleration regions at high densities that produce intense electron beams. High energy solar flares are the most common cause of such type III bursts.

The stopping frequency of type III bursts is equally as variable. Some type III bursts will only exist at high frequencies above 100 MHz. Such bursts are attributed to electron beams that are confined to the solar corona by a magnetic field with no access to the upper corona or the heliosphere (closed magnetic field). Other type III bursts can make it to kHz frequencies, going down to 10s of kHz or below, where 20 kHz corresponds to the plasma frequency near the Earth. Such bursts are considered interplanetary type III bursts. What frequency constitutes an interplanetary type III burst is not defined; as such a classification requires defining when the corona stops and interplanetary space starts. Certainly if a type III burst makes it to frequencies below 1 MHz (roughly a distance of 7 $R_\odot$) it should be considered "interplanetary". Interplanetary type III bursts are usually made up of a number of distinct type III bursts at high frequencies that cannot be differentiated at lower frequencies (see Fig. 1). Using spacecraft, Leblanc et al. (1995, 1996) analyzed the stopping frequency of type III radio bursts, finding that weaker radio bursts generally had higher stopping frequencies. What process causes the stopping frequency is not clear but Leblanc et al. (1995) hypothesize that it could be due to electron beam dilution and/or background density fluctuations.

2.1.2 Burst duration

The duration of individual type III bursts varies inversely as a function of frequency. Velocity dispersion of the electron beam exciter elongates the beam as a function of distance. As such the beam spends more time at lower frequencies. The rise and decay of type III radio emission in the inter-

planetary medium generally takes the form of a Gaussian total rise time t_e followed by a power-law e-folding decay time t_d. The general trend in emission is a shorter rise time $t_e < t_d$.

A statistical study of rise and decay time between 2.8 MHz and 67 kHz was undertaken by Evans et al. (1973). The study found with a least squares fit through the data the relations $t_e = 4.0 \times 10^8 f^{-1.08}$ and $t_d = 2.0 \times 10^8 f^{-1.09}$ where t is in seconds and f is in Hz. A similar result was found by Alvarez & Haddock (1973a) using a number of different studies in the frequency range 200 MHz to 50 kHz. They found a decay time $t_d = 10^{7.7} f^{-0.95}$. Rise and decay times that are roughly inversely proportional to frequency ($t_e \propto t_d \propto f^{-1}$) have been found at decimetric and microwave frequencies (Benz et al. 1983a; Staehli & Benz 1987). It is important to note here that the rise and decay times are proportional to each other (longer rise times lead to longer decay times). The power-law form of the decay time is currently unexplained as collisional damping of Langmuir waves would lead to a much longer decay time (e.g. Abrami et al. 1990). There must be another process which accounts for either the spatial damping of Langmuir waves or the suppression of Langmuir waves inducing electromagnetic emission. Harmonic emission is generally more diffuse in time, having a slower rise and decay time than fundamental emission for a given frequency (e.g. Caroubalos et al. 1974). Given the differences in the emission mechanisms, particularly the potential involvement of rapidly damped ion-sound waves in fundamental emission, this difference is unsurprising.

2.1.3 Frequency drift rate

The defining property of a type III radio burst in comparison to other solar radio bursts is their high drift rate df/dt (usually measured in MHz s^{-1}). Exactly how the frequency drift rate is calculated is subjective with some authors using the drift rate of the type III burst onset and some authors using the drift rate of the type III burst peak flux. One major survey of type III burst drift rate was done by Alvarez & Haddock (1973b) who used the rise time of type III bursts between 3 MHz and 50 kHz and combined them with eight other studies up to 550 MHz. They reported a least squares straight line fit to the frequency drift rate over all four orders of magnitude such that $df/dt = -0.01 f^{1.84}$. More recently a linear dependence ($df/dt \propto f$) was found for the frequency drift rate by Melnik et al. (2011) between the frequencies 30 MHz to 10 MHz for a number of powerful radio bursts occurring during a two month period in the solar maximum of 2002. The value of the frequency drift rate was similar at 10 MHz to Alvarez & Haddock (1973b) but smaller by a factor of two at 30 MHz. Going to higher frequencies, studies by Aschwanden et al. (1995a) and Meléndez et al. (1999) looked at radio bursts between 100 MHz and 3000 MHz and found drift rates $df/dt = 0.1 f^{1.4}$ and $df/dt = 0.09 f^{1.35}$ respectively. Again, these values differ from Alvarez & Haddock (1973b) but it must be noted here that Alvarez & Haddock (1973b) did not use very many points greater than 200 MHz in their study. Going to even higher frequencies, a recent study by Ma et al. (2012) looked at microwave type III bursts from 625 MHz to 7600 MHz, similar in range to events considered by Staehli & Benz (1987). Ma et al. (2012) found a much faster frequency drift rate, $df/dt = -2.6 \times 10^{-6} f^{2.7}$, in the range 635 MHz to 1500 MHz. Both studies quote varying values from hundreds to 17000 MHz s^{-1} at higher frequencies.

The drift rate of type III bursts can be used to estimate the speed of the exciting electron beam. Assuming a coronal (or interplanetary) density structure to obtain electron density as a function of distance $n_e(r)$, one can find frequency as a function of distance $f(r)$. Assuming either fundamental or harmonic emission (see Sect. 2.3.2), df/dt can be converted to $dr/dt = v$ as an estimation of the speed of exciting electrons. Derived exciter speeds for type III bursts are usually fractions of the speed of light and can range from $> 0.5\,c$ in the corona (Poquerusse 1994; Klassen et al. 2003) down to much slower velocities nearer to the Earth. Exciter speeds derived by Alvarez & Haddock (1973b) are fast, typically being $> 0.2\,c$. Exciter speeds derived by Aschwanden et al. (1995a) and Meléndez et al. (1999) are in the regime of $0.14\,c$ (7 keV). These are slower than the exciter speeds of Alvarez & Haddock (1973b), however, Meléndez et al. (1999) specifically state that they use the

maximum of type III emission and not the onset of type III emission. The latter would lead to higher drift rates and might explain some of the discrepancy between the studies. We expect the drift rate to be faster in the deep corona as the frequency of the background plasma is changing much faster with distance.

2.2 Flux and Size

2.2.1 Source flux

At a given frequency the distribution of source flux of type III bursts varies over many orders of magnitude. Statistically the distribution can be approximated as a power-law with a spectral index of 1.7 (Nita et al. 2002; Saint-Hilaire et al. 2013). This spectral index has been found at GHz frequencies and frequencies at 100s of MHz. It is the same spectral index that has been observed in X-ray flare energies (Crosby et al. 1993; Hannah et al. 2008). This spectral index is also seen in self-organized criticality (SOC) studies (e.g. Lu & Hamilton 1991; Aschwanden 2012).

Statistically, the peak source flux of type III bursts increases as a function of decreasing frequency in the corona. This increase goes up to roughly 1 MHz. On average the peak flux then decreases as a function of decreasing frequency (Weber 1978; Dulk et al. 1984, 1998). Exactly how the flux of individual type III bursts varies changes depending on the burst. Some bursts have been observed to peak as low as 0.1 MHz while others peak as high as 5 MHz (Dulk 2000). An example spectrum can be found in Dulk et al. (2001) showing a rise and decay of type III flux over two and a half orders of magnitude, starting around 50 MHz and ending at 20 kHz. Recently Saint-Hilaire et al. (2013) statistically examined type III burst source fluxes at 450 MHz to 150 MHz. By fitting the power-law distributions of source flux they found the normalization constants varied with frequency as $A \propto f^{-2.9}$. The increase in source flux as a function of decreasing frequency can be attributed to a number of factors including the increasing ease of generating Langmuir waves, the increasing velocity dispersion of the electron beam as a function of distance and the decrease in collisions.

2.2.2 Source size

The size of type III bursts increases with decreasing frequency. Measurements at various frequencies for a variety of bursts give averages (half widths to 1/e brightness) of $2'$ at 432 MHz, $4.5'$ at 150 MHz (Saint-Hilaire et al. 2013), $11'$ at 80 MHz, $20'$ at 43 MHz (Dulk & Suzuki 1980), $5°$ at 1 MHz, $50°$ at 100 kHz (Steinberg et al. 1985) and 1 AU at 20 kHz (plasma frequency near the Earth) (Lin et al. 1973). The electron beam exciter is guided by the solar/interplanetary magnetic field that expands as a function of distance from the Sun. As the background electron density (frequency) decreases as a function of distance from the Sun, type III burst source sizes increase at lower frequencies. The source sizes above 20 MHz are measured through ground based radio interferometers. Radio emission below 10 MHz does not typically make it through the ionosphere, so source sizes here are measured using the modulation factor of antenna signal due to spacecraft spin.

A comprehensive study of type III radio source sizes at low frequencies is undertaken by Steinberg et al. (1985) who deduces an f^{-1} variation of source angular size with observing frequency at frequencies below 2 MHz. This is directly proportional to the distance from the Sun implying expansion in a fixed cone of $80°$ with the apex in the active region. However, there was a correlation between the local plasma frequency and the source size. Scattering from density inhomogeneities in the background plasma expands the apparent source size and occurs within 0.2 AU at frequencies < 200 kHz. This results in expansion of the electron beam in a fixed cone of $30° - 40°$ with the apex in the active region. In the corona, Saint-Hilaire et al. (2013) also found an approximate f^{-1} variation from the mean observed size between 150 and 432 MHz over 10 yr of type III data using the Nançay Radioheliograph (NRH). They also fitted the high end of the source size dis-

tribution with a power-law in both size and frequency, finding that the normalization constant varied as $f^{-3.3}$. It is not obvious why the exponent has such a high magnitude but it could be related to multiple sources merging into one at lower frequencies, given the constraint of 10 s data required for such a huge study of radio bursts.

2.2.3 Brightness temperature

The brightness temperature T_b of a radio source is the temperature which would result in the given brightness if inserted into the Rayleigh-Jeans law. The brightness temperature can be measured with knowledge of the flux density and the source size and is a commonly used metric in radio astronomy. Type III bursts are characterized by their very large brightness temperatures that typically lie within the range 10^6 K to 10^{12} K although the brightness temperature can rise as high as 10^{15} K (Suzuki & Dulk 1985). For 10 years of NRH data, Saint-Hilaire et al. (2013) investigate the histogram of peak brightness temperatures within the range 150–450 MHz. They find that the brightness temperature at all six frequencies varies as a power-law with spectral index around -1.8 (larger T_b is less likely than smaller T_b). The brightness temperatures varied from 10^6 K to 10^{10} K with a few events $> 10^{11}$ K. At lower frequencies the trend is continued, with T_b increasing with decreasing frequency up to around 1 MHz and then either decreasing or remaining constant (Dulk et al. 1984). The decrease of T_b with decreasing frequency after 1 MHz cannot be explained due to increasing source size. There is also a weak anti-correlation between rise times and T_b. Fundamental type III emission is thought to produce higher T_b than harmonic emission (Dulk et al. 1984; Melrose 1989b), relating to both a larger flux density and a smaller source.

2.3 Scattering, Polarization and Harmonic Structure

2.3.1 Scattering

It is generally accepted that the source sizes of EM emission from the corona will be affected by scattering of radiation en route between source and observer. The rapid time variations in emission are inconsistent with a large source, and thus observations of higher frequency radio bursts with sizes of several arcminutes must be due to scattering. Additional motivation comes from the observations summarized by Bastian (1994), that no fine structure is observed in sources at scales below $20''$ at 1.5 GHz and around $40''$ at 300 MHz. Ray-tracing analyses have been used to study the effect in the context of type III emission (Steinberg et al. 1971; Steinberg 1972; Itkina & Levin 1992) and a comparable analytical approach was developed by Arzner & Magun (1999). For example Riddle (1972) showed that a point source at 80 MHz would be observed to be as large as $2'$, and the directivity of the radiation would be greatly reduced, particularly for fundamental emission, which is emitted into a relatively narrow cone.

A directivity study on 10 yr of data from 1995 to 2005 was done by Bonnin et al. (2008) using both the Ulysses and WIND spacecraft. They examined about 1000 type III bursts observed in the frequency range of 940 kHz to 80 kHz. They found that the radiation diagram axis shifts significantly to the east from the direction of the local magnetic field, similar to previous observations (Hoang et al. 1997), with this shift increasing for decreasing frequencies. They attributed this to a density compression when the fast and slow solar wind meet, resulting in a transverse density gradient that bends radiation in the eastward direction. They found no significant variation of directivity with solar activity or latitude.

2.3.2 Harmonic structure

In a large number of observed radio bursts both the fundamental (F) and harmonic (H) components are seen. Bursts above around 100 MHz generally do not show two separate components and the

observed component is thought to be the harmonic. Below 100 MHz both fundamental and harmonic emission are frequently seen (e.g. Wild et al. 1954; Stewart 1974; Dulk & Suzuki 1980; Suzuki & Dulk 1985; Robinson & Cairns 1994, 1998). Various theoretical estimates suggest that F emission is more common at large distances from the Sun, while the H component dominates closer, i.e. at higher frequencies (Robinson & Cairns 1994; Dulk et al. 1998). For emission at very high frequencies in the GHz and high MHz ranges, the absorption of radiation due to inverse bremsstrahlung becomes important. Under the assumption of a locally exponential density profile the optical depth is easily calculated (e.g. Karlicky 1998; Ratcliffe & Kontar 2014). The F emission is highly suppressed above around 500 MHz, while the harmonic is only affected above 1 GHz or so (e.g. Robinson & Benz 2000). In the 100–500 MHz range absorption is unimportant and cannot explain the rarity of F emission.

The H-F ratio, naively expected to be 2:1, actually ranges from 1.6:1 to 2:1 with a mean near 1.8:1 (Wild et al. 1954; Stewart 1974). This may be explained by propagation effects altering the initial ratio of 2:1. Simply put, for EM radiation in plasma the group velocity tends to zero as the frequency approaches the plasma frequency, but for frequencies much larger than ω_{pe} it tends to c. Thus the fundamental will be delayed relative to the harmonic emission from the same location (e.g. Dennis et al. 1984). On the dynamic spectrum, the F component will be shifted to later times and the H-F ratio is correspondingly reduced. The occasional instance of smaller ratios around 1.5:1 may suggest the two components are not F and H but rather the second and third harmonics (see e.g. Zheleznyakov & Zlotnik 1974; Brazhenko et al. 2012).

2.3.3 Polarization

Type III bursts are usually weakly circularly polarized with H emission having a lower degree of polarization than F emission (e.g. McLean 1971; Suzuki & Sheridan 1977; Dulk & Suzuki 1980; Suzuki & Dulk 1985). Dulk & Suzuki (1980) made a thorough analysis of polarization characteristics of 997 bursts, finding the average degree of polarization of F-H pairs was 0.35 and 0.11 respectively while structureless bursts only had a polarization of 0.06. The maximum F polarization was around 0.6. At high frequencies (164–432 MHz) polarization has been found to peak either before or simultaneously with the peak flux but never after it (Mercier 1990). Polarization was also found by Mercier (1990) to increase as a function of frequency, ranging from approximately 5% at 164 MHz to 15% at 432 MHz, in contrast to the results of Dulk & Suzuki (1980). Type III bursts with nearly 100% polarization have been observed at microwave frequencies (Wang et al. 2003). For solar emission, any linear polarization in the source tends to be obliterated over any finite band of frequencies by differential Faraday rotation of the plane of polarization during passage through the heliosphere (e.g. Suzuki & Dulk 1985).

Fundamental emission is generally produced very close to the plasma frequency and therefore below the X-mode cutoff. It would thus have polarization close to 1. Effects such as mode coupling due to magnetic fields (e.g. Zheleznyakov & Zlotnik 1964), and scattering due to low-frequency waves (Wentzel 1984; Melrose 1989a), or kinetic Alfvén waves (Sirenko et al. 2002) during propagation are certainly able to reduce the degree of polarization but cannot explain why fully polarized emission is never seen. Wentzel (1984) therefore proposed that the emission was depolarized to some extent within the source region itself, and that this was inherent to the emission process. For harmonic emission, it was initially thought that the Langmuir waves involved would coalesce head on, and therefore Melrose & Sy (1972); Melrose et al. (1978) and the correction by Melrose et al. (1980) concluded that harmonic emission must be weakly O-mode polarized. Later work by Willes & Melrose (1997) showed that relaxing the head-on condition allowed stronger polarization, with less restriction on the participating Langmuir waves.

2.4 Variants of Type III Bursts

2.4.1 Reverse and bi-directional type III bursts

Ordinary type III bursts are produced by an electron beam traveling outwards from the Sun, along the magnetic field, and drift from high to low frequency. Electrons traveling downwards into the solar atmosphere instead encounter plasma with increasing density, and thus drift from lower to higher frequencies. These radio bursts usually have a high starting frequency > 500 MHz (Isliker & Benz 1994; Aschwanden & Benz 1997; Robinson & Benz 2000) and fast drift rates due to the increased spatial gradient of the high density lower coronal plasma. In some cases a reverse drift and a normal drift burst are produced at the same time, from the same acceleration region, leading to a bi-directional burst. These are relatively uncommon, with the study of Meléndez et al. (1999) finding only 5% of bursts which extended above 1 GHz had both components in contrast to 66% which had a reverse slope component.

The general suggestion to overcome strong inverse bremsstrahlung damping during escape is that the emission arises in dense loops embedded in less dense surrounding plasma (Benz et al. 1992), which strongly increases the escaping fraction of radiation. Even in this case, it is likely to be only the harmonic component which may be observed (Chen et al. 2013a). Higher background densities increase the collisional rate and reduce the Langmuir wave growth rate. An increasing background plasma density reduces the level of Langmuir waves generated by an electron beam (e.g. Kontar 2001b). High frequency type IIIs are thus less frequent and dimmer. In the study of Meléndez et al. (1999) the peak fluxes were generally 10 sfu.

Recent simulations were carried out by Li et al. (2011c) for bi-directional electron beams producing type III radiation. As previously found from observations, they find that downward directed electron beams produce much less intense radio emission than upwards propagating electron beams. The fact that Meléndez et al. (1999) observe some instances of more intense emission in the reverse type III emission points towards an asymmetry for these events in the electron beam properties, like density. Li et al. (2011c) also find the background plasma properties are hugely important for allowing the emission at higher frequencies to escape the corona.

2.4.2 Type IIIb bursts

Frequency fine structures are commonly observed in type III bursts, and generally referred to as a type IIIb burst. Rather than the smooth emission of a "normal" type III, the emission is fragmented and clumpy. In general, it is the F component which shows this structure, and fine structure in the H component in type IIIb bursts is very rarely observed (Dulk & Suzuki 1980). Type IIIb bursts consist of a chain of emission bands, sometimes referred to as striae (de La Noe & Boischot 1972), each of which shows minimal frequency drift, whereas the chain as a whole drifts like a normal type III. de La Noe (1975) found that the bandwidth of the striae in the 20–80 MHz range was commonly around 60–100 kHz, similar to their frequency separations. More recent observations by Melnik et al. (2010) show similar bandwidths for the striae of 50 kHz, but found strong variations in their duration, flux and frequency drift as a function of the source position on the solar disk.

The common belief (Smith & Riddle 1975; Melrose 1980b, 1983; Li et al. 2012) is that density inhomogeneities in the background plasma create a clumpy distribution of Langmuir waves and are the cause of this fine structure. Harmonic emission, with its dependence on Langmuir wave backscattering, may be expected to show less modulation in this case. Fundamental emission, with its rapid growth and dependence on rapidly damped ion-sound waves, would be more susceptible. If density fluctuations are the cause then we may infer this is less intense closer to the Sun, leading to the absence of type IIIb's at higher frequencies.

Fine structure in the form of "sub-bursts," also in the decimeter range, was reported by e.g. Mel'Nik et al. (2005); Melnik et al. (2007). In this case, the main burst envelope shows weak emis-
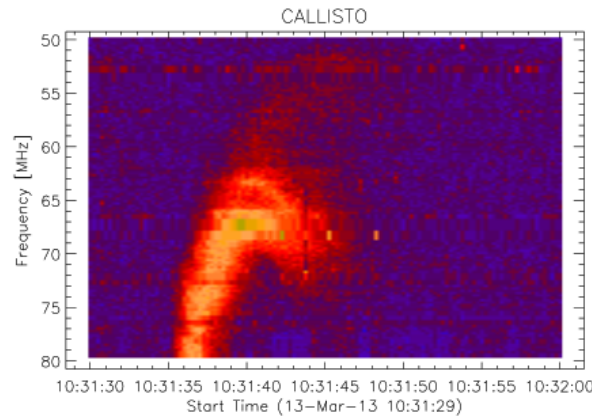
Fig. 3 An example of a type J burst from the Glasgow based e-Callisto spectrograph, 13th March 2013. Note the reversal in the frequency drift rate.

sion, and superposed on this are more intense stripes, with rapid frequency drifts on the order of 1 MHz s^{-1}, comparable to the main burst drift rate of around 3 MHz s^{-1}. These cannot be ascribed to density turbulence, and are as yet unexplained.

2.4.3 Type U and J bursts

The frequency drift rate of radio bursts has been observed to change sign during a normal type III burst, taking the shape of an inverted U or J (Maxwell & Swarup 1958) (Fig. 3). These bursts are believed to be electron streams traveling along magnetic fields confined to the corona (e.g. Klein & Aurass 1993; Karlicky et al. 1996). For the J bursts, the radio emission stops when the electron beam reverses direction but with U bursts it continues to higher frequencies. The rate of occurrence is very low and they generally occur in harmonic emission within the range 20–300 MHz, although fundamental emission has been observed (e.g. Labrum & Stewart 1970; Aurass & Klein 1997, and references therein). The rising and descending branches have spatially separated sources (Aurass & Klein 1997). Their polarization is usually below 10%, agreeing with the properties of harmonic emission. Similar to reverse drift bursts their low occurrence could be related to increased difficulties generating Langmuir waves in an increasing density gradient.

2.4.4 Type V bursts

Closely related to the type III burst are type V bursts, classified due to their long durations (minutes) and wide spectra (Wild et al. 1959). The type V emission appears as a continuation of a type III burst in the dynamic spectra. Type V bursts are important because their explanation has to be consistent with any model of type III bursts. Type V bursts appear at low frequencies below 120 MHz and generally have 1–3 minute durations (Dulk et al. 1980). The size of type V bursts increases rapidly with decreasing frequency, with full width at 1/e brightness on average 105 arcmin^2 at 80 MHz and 300 arcmin^2 at 43 MHz (Robinson 1977) similar to type III bursts (Dulk & Suzuki 1980). Type V bursts have also been observed to move relative to the disk surface at speeds ≈ 2 Mm s^{-1} (Weiss & Stewart 1965). A similar problem to type IIIs occurs for the decay of type V emission where the characteristic time of collisional damping of Langmuir waves is much larger than the lifetime of type V emission. Type V polarizations are low (usually $< 0.07\%$) which suggests harmonic emis-

sion. However, it is common to find their polarization is opposite to the sense of the corresponding type III. Dulk et al. (1980) suggest the most likely reason for this change is due to X-mode rather than O-mode emission. This could be caused by increased isotropy in the Langmuir wave distribution as the condition for O-mode emission is that the Langmuir waves lie within $20°$ of the magnetic field.

Another deviation of type V emission from their associated type III emission is the occurrence of large differences in position, sometimes up to 1 R_s (Weiss & Stewart 1965; Robinson 1977). This is not always observed and the positions of the type III and V can overlap or only be slightly displaced. One explanation of type V emission is low energy electrons traveling along different magnetic field lines or a variation in the beaming of emission changes the position of the centroids (Dulk et al. 1980). Another explanation given for type V emission is the electron-cyclotron maser instability (Winglee & Dulk 1986; Tang et al. 2013).

2.4.5 Type III-l bursts

Associated with coronal mass ejections (CMEs) and solar energetic protons are type III-l bursts (Cane et al. 2002; MacDowall et al. 2003). These bursts start at much lower frequencies than normal (hence the name type III-l), around 10 MHz, and progress to lower frequencies as a function of time. Moreover the bursts usually start delayed with respect to the associated flare and last on average 20 min. It has been suggested (Cane et al. 2002) that type III-l bursts are produced by electrons accelerated by reconnection behind fast CMEs. Conflicting accounts were found by MacDowall et al. (2009); Cliver & Ling (2009) as the former found type III-l events were associated with intense SEP events favoring flare acceleration of the CME, while the latter found type III-l events associated with type II bursts favoring shock acceleration of the CME. However, Gopalswamy & Mäkelä (2010) found that the presence of a type III-l burst does not always signify the presence of solar energetic protons.

2.4.6 Type III storms

A phenomenon called type III storms can occur when type III bursts are observed quasi-continuously over a period of days (Fainberg & Stone 1970a,b, 1971). These type III bursts are narrow-band and usually occur at low frequencies of < 100 MHz. An example of a type III storm over a six hour period is shown in Figure 4. Type III storms are usually observed as harmonic emission with a low degree of polarization. However, fundamental-harmonic pairs are observed in type III storms with the fundamental component having a higher polarization and is usually fragmented like a type IIIb burst (de La Noe & Boischot 1972). Type III storms have been associated with type I noise storms, a similar phenomenon at higher frequencies but with no frequency drift rate (a good review of type I storms can be found by Kai et al. 1985) which in turn are associated with a solar active region (e.g. Kayser et al. 1987; Gopalswamy 2004). The polarization degree of type III storms can remain constant during the entire length of the storm. Reiner et al. (2007) analyzed storms below 1 MHz and found only a 5% degree of polarization, different from the higher 25% polarization degree found for type III storms above 20 MHz by Kai et al. (1985). However, Reiner et al. (2007) found the polarization peaks near the central meridian crossing of the corresponding radio sources and decreases systematically with decreasing frequency. They deduced from these polarization measurements that the coronal magnetic field (at least above the active regions they study) does not fall off as $1/R^2$ but slower.

Type III storms usually consist of many faint type III bursts. Analyzing the flux distribution at two specific frequencies of 1.34 MHz and 860 kHz, Morioka et al. (2007) found the occurrence rate of type III storm emission obeyed a power-law distribution with spectral index of -3.7 and -3.6 respectively. Different spectral indices between -2.36 to -2.10 were found by Eastwood et al.
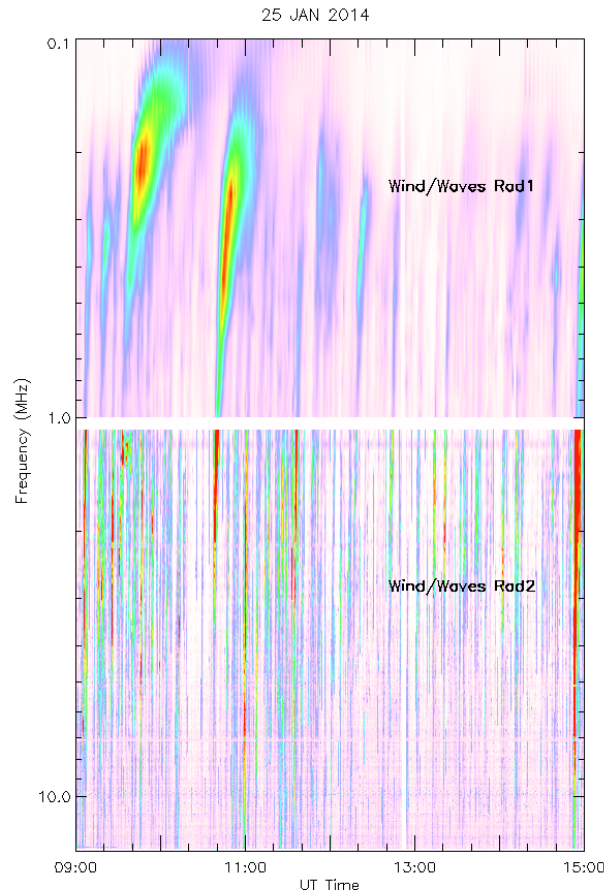
25 JAN 2014

Fig. 4 An example of a type III storm over a 6 h period observed by the WAVES experiment onboard the WIND spacecraft (Bougeret et al. 1995). This type III storm went on for a number of days.

(2010) at a number of different frequencies between 3 and 10 MHz. The discrepancy between the two ranges of indices is suggested by Eastwood et al. (2010) to be due to the averaging of a few storms and the use of data binning in Morioka et al. (2007). By comparison, the spectral index of flux occurrence rate of type I emission has been found to be -3 (Mercier & Trottet 1997).

2.5 Multiwavelength Studies

2.5.1 Type IIIs and X-rays

Type III radio bursts are not the only wavelength of light that can help diagnose the properties of accelerated electrons at the Sun. X-ray emission is frequently observed during solar flares and is believed to also be driven by accelerated electrons. Electrons travel into the dense solar chromosphere and thermalize via electron-ion Coulomb collisions. Bremsstrahlung X-rays are emitted (see Holman et al. 2011, as a recent review) and are detected both directly and through X-rays reflected from the solar surface (e.g. Kontar & Jeffrey 2010). We can use the X-ray signature to deduce the temporal, spatial and energetic profile of the energized electrons (e.g. Kontar et al. 2011).
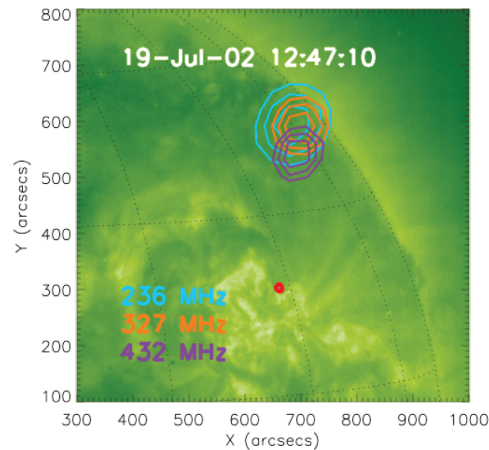
Fig. 5 An example flare imaged by RHESSI (Lin et al. 2002) at 12–25 keV in X-rays (*red*) and by the NRH (Kerdraon & Delouis 1997) at 432 MHz (*purple*), 327 MHz (*orange*), and 237 MHz (*blue*). All contours are at 10% intervals starting from 70 percent. The background is an EIT 195 Å.

The simultaneous observation of hard X-rays (HXR) and metric/decimetric radio emission is commonplace during flares and the relationship between type III bursts and hard X-ray emissions has been studied for many years (see for example Pick & Vilmer 2008, for a review). An example flare showing simultaneous X-ray and type III emission is shown in Figure 5. A recent study by Benz et al. (2005, 2007) on 201 flares above GOES class C5 found that nearly all flares were associated with coherent radio emission between the range 4 GHz to 100 MHz. The majority of flares in the study that had coherent radio emission had a type III burst or groups of type III bursts.

There have been many statistical studies between coherent type III radio emission and HXR bursts (e.g. Kane 1972, 1981; Hamilton et al. 1990; Aschwanden et al. 1995a; Arzner & Benz 2005). Bursts of type III radio emission have been found to temporally correlate with bursts in HXRs (e.g. Aschwanden et al. 1995b; Arzner & Benz 2005). However, there is often a small delay in the emission (e.g. Dennis et al. 1984; Aschwanden et al. 1995a) of 2 s or less. A type III/X-ray correlation is systematically more likely when the intensity of the HXR or radio emission increases (Kane 1981; Hamilton et al. 1990). Such a property could be the reason for the high association rate of $> C5$ GOES class flares found by Benz et al. (2005). A higher peak starting frequency of the type III bursts has also been found to be more likely in type III/HXR correlated events along with a low spectral index of HXRs (hard spectrum).

Recently, Reid et al. (2014) found a correlation between the starting frequency of type III bursts and the hard X-ray spectral index in flares. The hard X-ray spectral index is proportional to the spectral index of the accelerated electron beam. A higher spectral index means the electron beam will become unstable faster and is thus able to generate type III radio emission at lower heights and consequently higher starting frequencies. Reid et al. (2011, 2014) used the connection between type III starting frequency and HXR spectral index, first used by Kane et al. (1982); Benz et al. (1983a), to deduce the spatial characteristics of flare acceleration regions. They found the height of the acceleration region varied between 25 to 200 Mm with a mean of 100 Mm. The vertical extent of acceleration regions varied between 2 to 16 Mm with a mean of 8 Mm. Some heights are in good agreement with the height found from time-of-flight X-ray analysis (Aschwanden et al. 1998) but others are higher in the corona.

It should also be theoretically possible to observe hard X-rays associated with the type III producing electron beams in the upper corona. The background density is much lower and so emission is expected to be extremely faint (Saint-Hilaire et al. 2009). Since we have not detected such X-ray emission yet, Saint-Hilaire et al. (2009) estimate that the number of electrons escaping in type III producing electron beams must be $\leq 10^{34}$ electrons s^{-1} above 10 keV.

The effect of producing Langmuir waves alters the distribution of electrons (see Sect. 4). Such an effect has been studied in the context of a flare accelerated electron beam propagating down through the corona and into the dense chromosphere to generate X-rays (Emslie & Smith 1984; Hamilton & Petrosian 1987; McClements 1987b,a; Hannah et al. 2009; Zharkova & Siversky 2011; Hannah & Kontar 2011; Hannah et al. 2013). If an electron beam is accelerated high enough in the corona it can become unstable to Langmuir wave growth and the spectral index of the electron beam can be modified. The electron spectrum tends to flatten (decrease in magnitude) and the total amount of X-rays emitted is less. For strong plasma inhomogeneity, electrons can be re-accelerated to high energies (see Sect. 4) and the total amount of X-ray radiation emitted can be more than predicted with a simple collisional model (Hannah et al. 2013).

2.5.2 Type IIIs and EUV/X-ray jets

The joint observations of type III bursts and soft X-ray (SXR) jets have been studied by a number of different authors (Aurass et al. 1994; Kundu et al. 1995; Raulin et al. 1996). They found that the emission was co-spatial and the centroids of the type III bursts at different frequencies were aligned with the soft X-ray jet, indicating that particle acceleration is taking place when coronal jets occur. Jets that are correlated with type III bursts are also observed in extreme-ultraviolet (EUV) (e.g. Innes et al. 2011; Klassen et al. 2011; Chen et al. 2013c,a) and are commonly associated with ^{3}He-rich solar energetic electron events (Wang et al. 2006; Pick et al. 2006; Nitta et al. 2008). The jets in these studies frequently arose from the border of an active region and a coronal hole. A study involving EUV and X-ray jets where simultaneous type III bursts were observed (Krucker et al. 2011) found hard X-ray footpoints that strongly suggest reconnection with a closed and open magnetic field. Hard X-rays have recently been observed to accompany EUV jets (Bain & Fletcher 2009; Glesener et al. 2012) where type III bursts were also present. This further strengthens the case that acceleration of particles is present at the same time that thermal plasma is ejected from the solar corona in the form of a jet. Other evidence is the in-situ detection of electron spikes < 300 keV (Klassen et al. 2011, 2012) at 1 AU which are very closely temporarily correlated with type III bursts and EUV jets although there is a slight timing issue (see Sect. 3).

A recent paper by Chen et al. (2013a) has used the newly upgraded EVLA (Perley et al. 2011) to make images of a type III burst at frequencies between 1 GHz and 2 GHz that occurred at the same time as observations of an EUV jet and an HXR footpoint. From the images they infer that the acceleration site of the type III bursts is below 15 Mm in the solar corona and the electron beam travels along bundles of discrete magnetic loops into the high corona. Moreover, by using EUV images they deduce that the coronal loops that the type III producing electron beams are traveling along may be cooler and denser than the surrounding plasma. This dramatically helps the radio emission to escape and is similar to the scenario proposed by Benz et al. (1992) for allowing decimetric emission to escape the corona.

3 IN-SITU PLASMA OBSERVATIONS

3.1 Electron Beams

The first in-situ observations of energetic particles (van Allen & Krimigis 1965) opened up the non-electromagnetic window of flare accelerated particle observations. Since then solar energetic electron events have been found to be closely related observationally (e.g. Ergun et al. 1998; Gosling et al.

2003; Krucker et al. 2007) and theoretically to solar type III radio bursts, having a 99% association rate (Wang et al. 2012).

Impulsive electron events often extend to $\sim 1\,\mathrm{keV}$ (Lin et al. 1996) with some even extending down to the $\sim$0.1 to $1\,\mathrm{keV}$ energy range (Gosling et al. 2003). The presence of such low energy electrons favors injection sites high in the corona at altitudes $\geq 0.1 R_{\odot}$ as Coulomb collisions in the low solar atmosphere will cause low energy electrons to lose their energy. Electron time profiles generally show a rapid onset and also near time-of-flight velocity dispersion (e.g. Lin 1985; Krucker et al. 1999, 2007). Electrons also have a beamed pitch-angle distribution at lower energies of < 20 keV (e.g. Lin 1990; Wang et al. 2011) but can have very high pitch angle distributions at high energies of 300 keV.

A statistical study of 10 yr of solar energetic electron events using the 3D plasma and Energetic Particle (3DP) instrument (Lin et al. 1995) on the WIND spacecraft was carried out (Wang et al. 2012), finding nearly 1200 events between 1995 and 2005. They found an occurrence rate of solar electron events can be fitted as a power-law at 40 keV and 2.8 keV with a spectral index between 1.08–1.63 and 1.02–1.38 respectively, which changes every year. This power-law is smaller than the one associated with type III radio bursts (1.7) observed at the high frequencies by Saint-Hilaire et al. (2013). One possible reason could be due to the high electron background flux at low energies (Wang et al. 2012) obscuring events that could steepen the power-law dependence.

Solar impulsive electron events detected in-situ generally display broken power-law energy distributions with lower energies having harder spectra. Broken power-law distributions have been observed for some time (e.g. Wang et al. 1971) but their origin has remained ambiguous, being either a signature of the acceleration mechanism or a transport effect. A recent statistical survey was carried out by Krucker et al. (2009) on 62 impulsive events. They found the average break energy was ≈ 60 keV with averaged power-law indices below and above the break of $\delta_{\mathrm{low}} = 1.9 \pm 0.3$ and $\delta_{\mathrm{high}} = 3.6 \pm 0.7$ respectively. The power-law indices have an average ratio $\delta_{\mathrm{low}}/\delta_{\mathrm{high}}$ of 0.54 with a standard deviation of 0.09. The power-law indices also correlate with a coefficient of 0.74. The presence of the broken power-law can be replicated by simulating electron beam propagation to 1 AU and their interactions with Langmuir waves (see Sect. 4).

It is often believed that solar energetic electron events propagate scatter-free from the Sun to the Earth (e.g. Wang et al. 2006). The observed correlation between the spectral indices of energetic electrons at the Sun from X-ray data and the Earth from in-situ data (Lin 1985; Krucker et al. 2007) is often viewed as an additional support for scatter-free transport. However, the injection time of energetic electrons at different energies does not correspond to the inferred injection time by looking at the associated type III bursts (Krucker et al. 1999; Haggerty & Roelof 2002; Cane 2003; Wang et al. 2006, 2011; Kahler et al. 2011; Klassen et al. 2012). Low energy electrons (e.g. 10 keV) have an early arrival time while high energy electrons (e.g. 100 keV) have a late arrival time. The early arrival time could be due to pitch angle scattering (e.g. Tan et al. 2011) or electron interaction with Langmuir waves (Kontar & Reid 2009). It is not entirely clear what causes the later arrival time of the high energy electrons although an increased path length greater than 1 AU has been suggested (e.g. Kahler et al. 2011).

3.2 Langmuir Waves

In-situ observations of Langmuir waves associated with type III radio bursts were first taken by Gurnett & Anderson (1976, 1977) using the Helios spacecraft at around 0.5 AU. They found that the distribution of Langmuir waves is very clumpy in space. Observations at 1 AU came later using the ISEE-3 spacecraft (Lin et al. 1981). More recent observations of clumpy Langmuir waves show similar properties (e.g. Kellogg et al. 2009) using the time domain sampler in the WAVES instrument onboard the STEREO spacecraft (Bougeret et al. 2008). Recently, Ergun et al. (2008) modeled the localization of Langmuir wave packets as a superposition of Langmuir eigenmodes and this concept

has been worked on by other authors (e.g. Graham & Cairns 2013). There have been a number of recent works claiming to observe Langmuir wave collapse in the solar wind (e.g. Thejappa et al. 2012, 2013). However, other studies have analyzed the same events but using all three components of the electric field (Graham et al. 2012b,a) and found that the electric field is too weak for wave collapse to occur. Recently Vidojević et al. (2011); Vidojevic et al. (2012) analyzed the statistical distribution of Langmuir waves measured near 1 AU by the WIND spacecraft (Bougeret et al. 1995). By looking at the Langmuir wave distributions of 36 different electron beams with careful background subtraction they found that the distribution of Langmuir waves is more accurately modeled by a Pearson's system of distributions (Pearson 1895) and not by a log-normal distribution as previously thought.

3.3 Solar Wind Conditions

The plasma in the solar corona and the solar wind is a nonuniform, turbulent medium with density perturbations at various length scales (see e.g. Bruno & Carbone 2005, for a review). Observations of how this background plasma fluctuates is important for modeling the Langmuir wave generation of electron beams responsible for type III radio bursts.

In-situ measurements have been used to determine the density spectrum near the Earth and between 0.3 and 1 AU with *Helios* (Marsch & Tu 1990). The spectral slope at frequencies below 10^{-3} Hz were found to have a tendency to get smaller the closer the spacecraft got to the Sun in the fast solar wind. These results were further extended by Woo et al. (1995) using Ulysses remote sensing radio measurements for distances $< 40 R_\mathrm{s}$ which predicted the decrease in r.m.s. deviation of the density turbulence in the fast solar wind at wavenumber $k = 1.4 \times 10^6$ km^{-1}. The results for density turbulence in the slow solar wind (Marsch & Tu 1990; Woo et al. 1995) showed a constant level around 10% which was also found in the later study from Spangler (2002). More recently Chen et al. (2012, 2013b) have examined the slope of the electron density fluctuations power spectral density for 17 intervals of solar wind. They found a $-5/3$ power-law below $0.1\,k\rho_i$ where ρ_i is the proton gyroradius. Between 0.1 and $1\,k\rho_i$ the spectrum flattens to -1.1, in-line with other observations at 1 AU (e.g. Celnikier et al. 1983; Kellogg & Horbury 2005) and closer to the Sun (Coles & Harmon 1989; Coles et al. 1991). Between 3 and $15\,k\rho_i$, Chen et al. (2013b) report a steepening of the spectral index to -2.75.

Background solar wind electrons are not in thermal equilibrium with a Maxwellian distribution but exist in a quasi-thermal state, with electrons extending to much higher energies (Lin et al. 1972). Their velocity distribution function at all pitch angles is usually modeled using two convecting bi-Maxwellians, the core and the halo. A skewed distribution also exists in the fast solar wind parallel to the direction of the magnetic field. Known as the strahl, this high energy tail usually propagates away from the Sun and has a narrow pitch angle distribution between $10°$–$20°$ wide. Observations of the background solar wind electrons have shown that a kappa distribution can better model the solar wind (Maksimovic et al. 2005; Le Chat et al. 2010). The kappa distribution more accurately models the electron temperature while having fewer free parameters than the sum of two Maxwellians. Recently Li & Cairns (2014) used a kappa distribution when modeling type III radio bursts. They found that a kappa distribution leads to a type III burst that drifts with a faster velocity. The increased level of higher energy background electrons in the kappa distribution reduces the Langmuir waves that are generated by slower velocity electrons. As such we only observe radio emission generated by higher energy electrons (and hence higher velocity) in the beam. The corresponding type III burst has a higher drift rate in frequency space.

4 ELECTRON BEAM INTERACTION WITH LANGMUIR WAVES

The current generally accepted mechanism for type III burst generation is the plasma emission mechanism as described in the introduction. Since the original proposal of Ginzburg & Zhelezniakov (1958), large amounts of work have been invested in the development of this theory. However, due

to its complicated nature, the exact details are still not fully understood. Many analytical treatments of the various steps exist and these have been supplemented by numerical simulations in order to develop the general picture of type III burst production as presented here.

The generation process is summarized in Figure 2. In this section we discuss the electron propagation and the resulting Langmuir wave generation. The evolution of the Langmuir waves via non-linear scattering and wave-wave interactions is the topic of Section 5 along with the processes that lead to second harmonic emission (at twice the local plasma frequency) and fundamental emission (first harmonic) at the local plasma frequency.

4.1 Quasi-linear Theory

The rapid frequency drift (see Sect. 2.1) of type III bursts is caused by the rapid motion of the generating electrons, and can be derived from a prescribed plasma density profile by assuming that the electrons stream freely (e.g. Karlicky et al. 1996; Robinson & Benz 2000; Ledenev et al. 2004). Alternatively, assuming a constant velocity for the exciting electrons we can derive the density profile of the ambient plasma (e.g. Cairns et al. 2009). However, the electrons do not stream freely but produce Langmuir waves. Early numerical simulations by e.g. Takakura & Shibahashi (1976); Takakura (1982) showed that Langmuir wave generation must be considered to reproduce the electron behavior over long distances, and therefore even the basic properties of type III bursts.

The quasi-linear equations describing the interaction of electrons with Langmuir waves were introduced by Vedenov et al. (1962); Drummond & Pines (1962). The 1-D version of these is often employed in relation to type III bursts, as we may assume the generating electrons are closely tied to the solar magnetic field, as has been observed in-situ near the Earth (Sect 3). Additional effects are seen in 2-d modeling (e.g. Ziebell et al. 2008a,b; Pavan et al. 2009a,b; Ziebell et al. 2011, 2012) such as heating of the background plasma (e.g. Yoon et al. 2012a; Rha et al. 2013). However the 1-d dynamics are generally expected to dominate.

Writing the electron distribution function as $f(v,t)$ [electrons cm^{-4} s], normalized so that $\int f(v,t)dv = n_e$ with n_e, the plasma density, in cm^{-3} and the spectral energy density of Langmuir waves as $W(v,t)$ [erg cm^{-2}] with the normalization $\int W(v,t)\,dv = E_L$, the total energy density of the waves in erg cm^{-3}, we have

$$\frac{\partial f(v,t)}{\partial t} = \frac{4\pi^2 e^2}{m_e^2}\frac{\partial}{\partial v}\frac{W}{v}\frac{\partial f(v,t)}{\partial v}, \tag{1}$$

$$\frac{\partial W}{\partial t} = \frac{\pi\omega_{pe}}{n_e}v^2 W\frac{\partial f(v,t)}{\partial v}, \tag{2}$$

where v signifies the electron kinetic velocity and the Langmuir wave phase velocity, as these must be equal for the interaction to occur. This is equivalent to the Cherenkov resonance condition that the wave's wavenumber k, frequency ω and the particle velocity v must satisfy $\omega = kv$.

The quasilinear equations are derived from the Vlasov equation by ignoring all other electromagnetic processes present in the plasma such as collisions. Several assumptions are needed, such as the absence of particle trapping, and the non-magnetization of the electrons, so that their gyroradius is large and their trajectories almost linear. We also need the weak-turbulence condition which states that the energy in Langmuir waves is much less than that in the background plasma. Provided the perturbations created on a particle through wave-particle interactions are small (for example much less than an electron gyroradius in a gyroperiod), the quasilinear equations are valid.

The growth rate of waves is (among other things) proportional to $\partial f/\partial v$ (Eq. (2)). When the electron distribution has a positive gradient in velocity space, we excite waves and vice versa. An intuitive way to understand this is as follows. The energy exchange between the particles and waves occurs for particles with speeds v close to ω/k; particles with $v < \omega/k$ gain energy from the waves
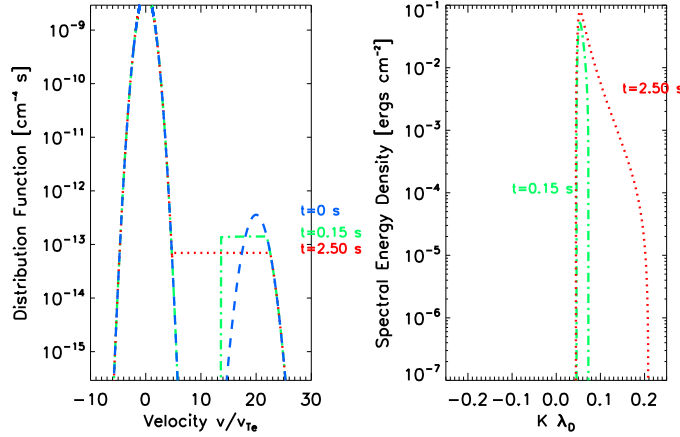
Fig. 6 A demonstration of an electron beam inducing Langmuir waves in the background plasma. *Left*: the electron distribution function of a background Maxwellian and an electron beam in velocity space (normalized by the thermal velocity v_{Te}. The density ratio is $n_{\mathrm{b}}/n_{\mathrm{e}} = 10^{-4}$ and $v_{\mathrm{Te}} = 5.5 \times 10^{8}$ cm s^{-1}. *Right*: the spectral energy density of Langmuir waves where the x-axis is normalized by the Debye length. The three different colors correspond to different points in time.

while particles with $v > \omega/k$ lose energy from the waves. The waves gain energy if we have more particles satisfying $v > \omega/k$ and the waves lose energy if we have more particles satisfying $v < \omega/k$.

The effect of wave generation on the electron distribution is more than simple energy loss. The right hand side of Equation (1) is a diffusion equation, with the diffusion operator $D = W/v$. The transfer of energy from electrons to waves and back to the electrons causes the electrons to diffuse in velocity, smoothing out the positive gradient and slowing the energy transfer. The asymptotic (long time) solution to the quasi-linear equations is thus a plateau in velocity space (e.g. Vedenov & Ryutov 1972; Grognard 1985; Kontar 2001c).

Figure 6 shows an example of the resonant interaction of Langmuir waves with electrons, and the resulting quasi-linear relaxation. The left panel shows the electron distribution consisting of a background Maxwellian plasma (density n_{e}) and an electron beam (density n_{b}) with a density ratio of $n_{\mathrm{e}}/n_{\mathrm{b}} = 10^{-4}$. The right panel shows the spectral energy density of Langmuir waves. This initial beam has a positive gradient in velocity, and so is unstable to Langmuir wave growth. After a short time (0.15 s) the electrons have excited a high level of Langmuir waves, and the beam has diffused in velocity, becoming significantly wider in velocity space. At a later time (2.5 s) the electron distribution has relaxed to a plateau with zero gradient in velocity space, and the instability has therefore saturated. The level of induced Langmuir waves has grown, as has their width in wavenumber space.

4.2 Distance for Electron Beam Instability

The electrons accelerated during a solar flare are generally expected to have a power-law like distribution in velocity with a negative index. Such a distribution will not generate Langmuir waves. However, time-of-flight effects, where fast electrons outpace slower ones, produce a distribution with positive slope which is unstable to Langmuir wave generation. This occurs only after the electrons have traveled a sufficient distance. This instability distance is closely related to the starting frequency of type III bursts. When the instability distance is small, the electron beam will produce Langmuir waves (and hence radio emission) close to the dense acceleration site resulting in a high burst starting frequency. When the instability distance is large, the electron beam travels into much

lower density plasma before exciting Langmuir waves and so produces type III emission that starts at lower frequencies.

Reid et al. (2011) modeled the distance that an instantaneously injected electron beam would travel for a range of parameters. They found that the size of the acceleration region and the spectral index of the electron beam were the dominating factors in calculating the starting frequency of the type III burst given a fixed height for the acceleration region. Low spectral indices and small acceleration regions reduce the distance for electron beam instability. Such a dependency was used by Reid et al. (2011, 2014) to deduce heights and sizes of flare acceleration regions (see Sect. 2.5). If the electrons are injected over a finite time (rather than instantaneously), the starting frequency will be affected (Reid & Kontar 2013). The longer the injection time is, the further the beam must travel to become unstable.

4.3 Persistence of the Electron Beam

In the early 60s, Sturrock (1964) noted that without something stopping the beam-plasma instability, the rate of Langmuir wave generation by an electron beam in the solar corona was enough that the beam would lose all energy after propagating only meters. However, observations of type III bursts showed that beams could persist to distances of 1 AU. The *beam-plasma structure* was proposed to overcome this: here the electrons propagate accompanied by Langmuir waves which are continually generated at the front of the beam and reabsorbed at the back (e.g. Zheleznyakov & Zaitsev 1970; Zaitsev et al. 1972; Mel'Nik 1995). Numerical work by e.g. Takakura & Shibahashi (1976); Magelssen & Smith (1977); Kontar' et al. (1998); Mel'Nik et al. (1999) confirmed that the beam-plasma structure could resolve the problem.

Other processes can suppress the beam-plasma instability and therefore the Langmuir wave growth. In particular, density fluctuations in the plasma can shift Langmuir waves out of resonance with the electrons (e.g. Smith & Sime 1979; Muschietti et al. 1985). Because the growth rate of Langmuir waves is proportional to their current level at a given wavenumber, this can suppress the instability (in line with Kontar 2001b; Ledenev et al. 2004; Li et al. 2006b; Reid & Kontar 2010). The density fluctuations can be either wave modes with wavelengths comparable to the Debye length (Vedenov et al. 1967; Goldman & Dubois 1982; Yoon et al. 2005), or longer wavelength inhomogeneities (Ryutov 1969; Nishikawa & Riutov 1976; Smith & Sime 1979; Kontar 2001a; Kontar et al. 2012). In the latter case, the Langmuir wave evolution can be described in the WKB approximation by (e.g. Ryutov 1969; Kontar 2001b)

$$\frac{\partial W}{\partial t} - \frac{\partial \omega_{\mathrm{pe}}}{\partial x}\frac{\partial W}{\partial k} = 0 \tag{3}$$

and as the plasma frequency is $\omega_{\mathrm{pe}} \propto \sqrt{n_{\mathrm{e}}}$, even weak density gradients are seen to strongly affect Langmuir waves.

For a propagating beam-plasma structure, density fluctuations will lead to energy loss, because when Langmuir waves are shifted out of resonance with the beam, their energy can no longer be reabsorbed. Recent numerical simulations (Kontar & Reid 2009; Reid & Kontar 2010, 2013) taking into account (among other processes) the refraction of Langmuir waves found that the beam does lose energy but is still able to persist over distances of 1 AU or more. Additionally, a power-law electron spectrum injected at the Sun was found by Kontar & Reid (2009) to be modified by density fluctuations and further from the Sun is better modeled as a broken power law (Reid & Kontar 2013). This is due to the combination of Langmuir wave generation and their spectral evolution. Additionally, the spectral evolution of Langmuir waves to small wavenumbers can in some circumstances lead to acceleration of high-velocity electrons in the tail of the electron distribution, because the Langmuir waves can transfer energy from the beam electrons into this tail. This effect has been studied nu-

merically by e.g. Kontar (2001b); Reid & Kontar (2010); Ratcliffe et al. (2012); Voshchepynets & Krasnoselskikh (2013); Krafft et al. (2013).

4.4 Langmuir Wave Clumping

Plasma density fluctuations are also believed to be responsible for the clumpy Langmuir wave distribution observed in-situ near the Earth. Background density fluctuations are known to correlate to the clumpy observations of Langmuir waves in the solar wind (Robinson et al. 1992). Recent simulations of the effects of density fluctuations on type III emission were carried out by Li et al. (2012). They considered a plasma density profile with several density enhancements and found these produced strong fine structure in both the fundamental and the harmonic component that resemble stria bursts. However, the fundamental component in these simulations is very weak and thus unobservable. The effect of temperature variation has also been investigated both for the electron temperature (Li et al. 2011b) and the ion temperature (Li et al. 2011a). Variations only in electron temperature (Li et al. 2011b) produced similar results to those presented for density fluctuations, although in general the emission was less intense. Interestingly, large fluctuations in the ion temperature (Li et al. 2011a) were able to produce more distinct fluctuations in the fundamental component and flux levels were able to reach 1 sfu. It is desirable to observe fragmented fundamental emission because the polarization of type IIIb bursts is usually observed to be quite high (see Sect. 2.3.3). The characteristics of the fine structures in these simulations resemble striae and thus density and/or temperature fluctuations are a promising explanation, although they cannot as yet explain the occurrence of normal H and modulated F pairs.

An alternative way to deal with density fluctuations was introduced by Robinson (1992); Robinson et al. (1992) called 'Stochastic Growth Theory' (SGT). The main principle behind SGT is that density fluctuations induce random growth of Langmuir waves. The bursts of Langmuir waves have an amplification factor of $\exp G$ where G is a random function with zero mean value and non-zero standard deviation. This predicts a log-normal statistical distribution of the electric field amplitude. SGT has been used with a variety of different simulation techniques (e.g. Robinson & Cairns 1998; Cairns & Robinson 1999; Li et al. 2006b,a) and has produced simulation results that resemble the clumpy observations of Langmuir waves and synthetic spectra of type III bursts.

Although quasilinear theory is very good at capturing the large scale effects of the electron beam - Langmuir wave interaction, it struggles to capture the small scale effects of single wave packets. An alternative approach can be used to model these small scales using the Zakharov equations (Zakharov 1972). This approach models the electric field with an additional source term to describe particles in the beam (e.g. Zaslavsky et al. 2010; Krafft et al. 2013). Modeling in this way is able to replicate wave clumping and thus strongly varying electric fields that have been observed in the solar wind (e.g. Ergun et al. 2008). It is also able to describe the reflection of Langmuir waves in density cavities where small scale lengths are important and the quasilinear approach is invalid.

5 NONLINEAR PROCESSES AND LANGMUIR WAVE EVOLUTION

As discussed in the introduction, many years of work have been invested in understanding the plasma emission mechanism. However, due to its complex nature, and the many interconnected processes, there are still many unanswered questions. One key feature of the mechanism is the nonlinear processes which control the evolution of the Langmuir waves, and their conversion into radio waves. While their details are complicated, the basic equations provide insight into emission properties such as brightness temperature and angular distribution and show us what plasma properties are important (e.g. temperature ratio). In this section, we will present the basic theory describing these processes. The derivation of the relevant equations is complicated, and is given in detail in the books by Melrose (1980a); Tsytovich (1995) and in many papers. Here, we only give a short introduction, and then focus on the application of the nonlinear equations to the problem of type III burst generation.

5.1 The General Form of the Nonlinear Equations

The density fluctuations in the previous section were generally considered to have scale lengths larger than the Langmuir wavelength. However, density-perturbing wave modes such as ion-sound waves can have wavelengths comparable to Langmuir waves. In this case, we can describe their effects as wave-wave interactions using a set of nonlinear equations. The scattering of Langmuir waves by individual plasma particles is also described using nonlinear equations. Both of these processes are vital for the further evolution of beam-generated Langmuir waves.

The key principle is "detailed balance;" in short we have interactions of the form $\sigma \rightleftarrows \sigma' + \sigma''$ where σ, σ' and σ'' denote wave modes, which can be the same, or different, and/or $\sigma + i \rightleftarrows \sigma' + i'$, where i and i' are an initial and scattered plasma ion respectively. For every wave we lose on the left hand side, we must gain a wave on the right hand side. Using this principle we can write down the rates of change of the "occupation number" of waves in mode σ. This is given by[1] $N_\sigma = (2\pi)^3 W_\sigma / \omega_\sigma$ where W_σ is the spectral energy density. The probability of an interaction is then calculated from the detailed plasma physics, and requires that we specify the exact modes involved.

Writing $\boldsymbol{k}, \omega, \boldsymbol{k}', \omega'$ for the wavevector and frequency of mode σ, σ' respectively, the ion scattering process $\sigma + i \rightleftarrows \sigma' + i'$ is described by the equation

$$\frac{dW_\sigma(\boldsymbol{k})}{dt} = \int \frac{d\boldsymbol{k}'}{(2\pi)^3} w_i^{\sigma\sigma'}(\boldsymbol{k}', \boldsymbol{k}) \left[\frac{\omega}{\omega'} W_{\sigma'}(\boldsymbol{k}') - W_\sigma(\boldsymbol{k}) - \frac{(2\pi)^3}{k_B T_i} \frac{\omega - \omega'}{\omega'} W_\sigma(\boldsymbol{k}) W_{\sigma'}(\boldsymbol{k}') \right] \quad (4)$$

with probability $w_i^{\sigma\sigma'}$ depending on the wave modes involved, and a second equation with the same probability and σ and σ' interchanged. The plasma ion absorbs the momentum change between the initial and final waves, and in the cases considered here this change is sufficiently small that we may neglect the effect on the ions.

For the process $\sigma \rightleftarrows \sigma' + \sigma''$, the equations take the form

$$\begin{aligned}
\frac{dW_\sigma(\boldsymbol{k})}{dt} &= \omega \int \int d\boldsymbol{k}' d\boldsymbol{k}'' w_{\sigma\sigma'\sigma''}(\boldsymbol{k}, \boldsymbol{k}', \boldsymbol{k}'') \\
&\times \left[\frac{W_{\sigma'}(\boldsymbol{k}')}{\omega'} \frac{W_{\sigma''}(\boldsymbol{k}'')}{\omega''} - \frac{W_\sigma(\boldsymbol{k})}{\omega} \left(\frac{W_{\sigma'}(\boldsymbol{k}')}{\omega'} + \frac{W_{\sigma''}(\boldsymbol{k}'')}{\omega''} \right) \right],
\end{aligned} \quad (5)$$

where $w_{\sigma\sigma'\sigma''}(\boldsymbol{k}, \boldsymbol{k}', \boldsymbol{k}'')$ is the emission probability. Equations for the other wave modes are similar, having the same probability but some sign changes.

The growth of mode σ occurs due to the product term (the first term in the square brackets) and the decay of this mode depends on both its own energy density and those of the decay products, giving the other two terms. So for example, if we start with a high level of mode σ and thermal levels of σ', σ'', that is, the level generated spontaneously by plasma particles, the interaction $\sigma \rightleftarrows \sigma' + \sigma''$ will proceed to the right, generating the modes on the right hand side, from that on the left hand side. Eventually, we can reach the state where $dW_\sigma / dt = 0$ and the interaction is saturated.

Along with Equation (5), we have some conservation conditions. Energy conservation in this equation may be expressed by the condition

$$\omega^\sigma(\boldsymbol{k}) = \omega^{\sigma'}(\boldsymbol{k}') + \omega^{\sigma''}(\boldsymbol{k}''), \quad (6)$$

where ω^σ is the frequency of a wave in mode σ, and is included to emphasize that we must consider the relevant dispersion relation for the mode in question. Momentum conservation is given by

$$\boldsymbol{k} = \boldsymbol{k}' + \boldsymbol{k}'' \quad (7)$$

---

[1] This definition varies slightly between authors. In Melrose (1980a) a factor $\hbar$ appears explicitly, and the $(2\pi)^3$ is omitted with corresponding changes in the quoted probabilities. Tsytovich (1995) uses the given definition.

for $\boldsymbol{k}, \boldsymbol{k}', \boldsymbol{k}''$ the respective wave vectors. For a 3-wave interaction to be possible we must be able to simultaneously solve energy and momentum conservation using the relevant dispersion relations (frequency-wavevector relations), e.g. those for Langmuir and EM waves

$$\omega_L(\boldsymbol{k}) \simeq \omega_{\mathrm{pe}} + 3v_{T_\mathrm{e}}^2 k^2/(2\omega_{\mathrm{pe}}), \qquad \omega_{\mathrm{EM}}(\boldsymbol{k}) = (\omega_{\mathrm{pe}} + c^2 k^2)^{1/2} \qquad (8)$$

respectively. Thus for example, the interaction $L + s \rightleftarrows L'$ is allowed, but $L + L' \rightleftarrows L''$ is not, as the resulting wave vector must be larger than k_{De}, and this is not possible for Langmuir waves.

5.2 Nonlinear Langmuir Wave Evolution

For Langmuir wave evolution, the probability used in Equation (4) for the scattering $L+i \rightleftarrows L'+i'$ is

$$w_i^{LL'} = \frac{\sqrt{\pi}\omega_{\mathrm{pe}}^2}{2n_\mathrm{e}v_{Ti}(1+T_\mathrm{e}/T_i)^2} \frac{|\boldsymbol{k}\cdot\boldsymbol{k}'|}{kk'|\boldsymbol{k}-\boldsymbol{k}'|} \exp\left(-\frac{(\omega'-\omega)^2}{2|\boldsymbol{k}'-\boldsymbol{k}|^2 v_{Ti}^2}\right). \qquad (9)$$

Due to the dot product, this probability is dipolar, i.e. it is maximized for $\boldsymbol{k}'$ either parallel or antiparallel to $\boldsymbol{k}$. The exponential term implies $\omega' \simeq \omega$ and so $|\boldsymbol{k}'| \simeq |\boldsymbol{k}|$. Finally, the appearance of $|\boldsymbol{k}-\boldsymbol{k}'|$ in both the exponential and main term implies that we mainly get backscattering, so that $\boldsymbol{k}' \simeq -\boldsymbol{k}$.

In Equation (4), the first two terms in the square brackets may be called spontaneous scattering, and give approximately linear growth or decay. Conversely, the third term depends on the spectral energy density already present. Because of the factor $\omega - \omega'$, the scattered waves will grow where $\omega' < \omega$, and decay where $\omega' > \omega$. Thus the main growth occurs for $\boldsymbol{k}' \simeq -\boldsymbol{k} + \Delta\boldsymbol{k}$ with the small decrement $\Delta\boldsymbol{k}$.

The main three-wave process affecting the Langmuir waves is $L \rightleftarrows L' + s$ where s denotes an ion-sound wave, with the approximate dispersion relation

$$\omega = kv_\mathrm{s}, \qquad v_\mathrm{s} = \sqrt{\frac{k_B T_\mathrm{e}}{M_i}\left(1+\frac{3T_\mathrm{i}}{T_\mathrm{e}}\right)}, \qquad (10)$$

for the sound speed. The probability for this process which appears in Equation (5) is

$$w_{LLs}(\boldsymbol{k},\boldsymbol{k}',\boldsymbol{k}'') = \frac{\pi\omega_{\mathrm{pe}}^2}{4n_\mathrm{e}T_\mathrm{e}}\left(1+\frac{3T_\mathrm{i}}{T_\mathrm{e}}\right)\omega_k^s\left(\frac{(\boldsymbol{k}'\cdot\boldsymbol{k}'')^2}{k'^2 k''^2}\right)\delta(\omega_{k'}^l - \omega_{k''}^l - \omega_k^s). \qquad (11)$$

Solving the energy and momentum conservation equations (Eqs. (6) and (7)) simultaneously using the appropriate wave dispersion relations tells us that the produced Langmuir wave has a wavevector approximately anti-parallel to the initial one, i.e. $\boldsymbol{k}'' \simeq -\boldsymbol{k}'$. The ion-sound wave must then have $\boldsymbol{k} \simeq 2\boldsymbol{k}'$. Thus as in the previous case of ion-scattering, we mainly generate backscattered Langmuir waves.

Again, rather than exact backscattering, the final Langmuir wavenumber has a slight decrement, so we have $k'' = -k' + \Delta k$ with

$$\frac{\Delta k}{k_{De}} = \frac{2}{3}\sqrt{\frac{m_\mathrm{e}}{m_i}}\sqrt{1+\frac{3T_i}{T_\mathrm{e}}} \sim \frac{1}{30}. \qquad (12)$$

Thus repeated Langmuir wave scatterings produce waves at progressively smaller wavenumbers, and can lead to significant spectral evolution. This can be important for the electromagnetic emission processes as there can be strong constraints on the participating wavenumbers.

A thermal level of ion-sound waves is naturally present in plasma and the high levels of Langmuir waves generated by an electron beam can produce rapid growth of ion-sound waves and

scattered Langmuir waves. However, ion-sound waves are subject to Landau damping with damping coefficient

$$\gamma_k^s = \sqrt{\frac{\pi}{8}} \omega_k^s \left[\frac{v_{\rm s}}{v_{T_{\rm e}}} + \left(\frac{v_{\rm s}}{v_{T_{\rm i}}} \right)^3 \exp - \left(\frac{v_{\rm s}}{v_{T_{\rm i}}} \right)^2 \right]. \tag{13}$$

In plasma with $T_{\rm i} \simeq T_{\rm e}$ this is very strong, approaching the ion-sound wave frequency, and thus the three-wave processes become inefficient. Referring to Equation (5), we see that this is because the positive "driving" term for the decay process is proportional to $W_{\rm s}$ and with strong damping this quantity remains small.

5.3 Harmonic Emission Equations

Because the temperature ratio in the solar corona and wind can vary (e.g. Newbury et al. 1998; Gurnett et al. 1979) from $T_{\rm i}/T_{\rm e} \lesssim 0.1$ to 1 or even 2, the ion-scattering and ion-sound wave decay processes described in the previous section vary in efficiency, with the latter dominating where the ratio is lower, and the former where it is large. However, in both regimes, we can produce a large level of Langmuir waves oppositely directed to the initial beam-generated population, and thus efficiently produce radiation at the second harmonic of the plasma frequency.

The growth rate for harmonic emission by the process $L + L' \rightleftarrows t$ is again given by Equation (5), with a probability

$$w^{LLT}(\boldsymbol{k}_1, \boldsymbol{k}_2, \boldsymbol{k}_T) = \pi \omega_{\rm pe} \frac{(k_2^2 - k_1^2)^2 (\boldsymbol{k}_T \times \boldsymbol{k}_1)^2}{16 m_{\rm e} n_{\rm e} k_T^2 k_1^2 k_2^2} \delta(\omega_{k_T}^T - \omega_{k_1}^L - \omega_{k_2}^L), \tag{14}$$

where we have labeled the participating Langmuir wavevectors as k_1, k_2 for clarity.

Using the energy and momentum conservation conditions (Eqs. (6) and (7)) and the dispersion relations (Eq. (8)) we find that the coalescing Langmuir waves must be approximately oppositely directed. This is referred to as the "head-on approximation" (HOA), and allows us to simplify the probability, by replacing $(k_2^2 - k_1^2)^2/k_2^2 = (\boldsymbol{k}_T \cdot \boldsymbol{k}_1)^2/k_1^2$.

To derive this, we must assume that $k_T \ll k_1, k_2$. For typical beam electrons, with $v \simeq 10 v_{T_{\rm e}}$ the generated Langmuir waves have $k \simeq 0.1 k_{De}$ and from $(\omega_{\rm pe}^2 + c^2 k_T^2)^{1/2} \simeq 2\omega_{\rm pe}$ we have that $k_T \simeq \sqrt{3}\omega_{\rm pe}/c$. The ratio k_T/k_1 is then of the order 0.2, which is not very small. Clearly then the coalescence is not perfectly head on.

Some simple calculations using Equation (14) can show that even accounting for the angle between k_1 and k_2, the most probable angle between k_1 and k_T remains close to 45°. More detailed calculations by e.g. Melrose & Stenhouse (1979); Willes et al. (1996); Willes & Melrose (1997) used specific angular distributions for the Langmuir waves to find the emission probability with and without applying the HOA. Significant differences were found at small wavenumbers. Thus the detailed study or simulation of harmonic emission is complicated. It must either be treated using a fully 3-dimensional model, or by analytically averaging over angles.

There are however two great simplifications which may be made to the equations for harmonic emission without affecting the results obtained. The energy lost from the Langmuir waves is very small, and so can be neglected when considering the evolution of Langmuir waves. The high group velocity of the EM waves, given by

$$\boldsymbol{v}_{\rm g} = c^2 \boldsymbol{k}/\omega \tag{15}$$

and approximately equal to c for emission at $2\omega_{\rm pe}$, means the emission rapidly leaves the source region where Langmuir waves are present. Thus the reverse process of $t \to L + L'$ can often be ignored, leaving only a growth rate of $dW_{\rm harmonic}/dt \propto W_L$ and W_L' for W_L and W_L', the beam generated and backscattered Langmuir wave populations respectively. Balancing this emission rate with the propagation losses from the source, we can find the approximate temperature where the

emission saturates. This depends on the beam and plasma parameters as well as the source model, but is usually many orders of magnitude above thermal and easily able to explain the observed brightness temperatures.

5.4 Equations Describing Fundamental Emission

For emission at the fundamental of the plasma frequency, we have two possible processes, analogous to those for Langmuir waves, namely the scattering by plasma ions, and the decay involving ion-sound waves. Ion-scattering was proposed in the original version of the plasma emission mechanism by Ginzburg & Zhelezniakov (1958). The three-wave processes are generally faster, but if the ion-sound wave damping is very strong, they are suppressed. For kHz wavelengths, i.e. plasma emission in the solar wind, often the ion-temperature is low, so the three-wave processes are fast, and as shown by Thejappa et al. (1993) ion-scattering is too slow to explain the observed brightness temperatures. It is however sufficient in the corona, as shown by Mel'Nik & Kontar (2003).

The processes are the scattering of a Langmuir wave into an electromagnetic wave, $L+i \rightleftarrows t+i'$, and two processes involving ion-sound wave interactions, namely $L + s \rightleftarrows t$, $L \rightleftarrows t + s$. The latter was proposed by e.g. Lin et al. (1986) as the most likely generating process for ion-sound turbulence in solar wind, but it is now generally thought that Langmuir wave decay $L \rightleftarrows L' + s$ produces the ion-sound waves and these drive the production of fundamental electromagnetic emission (Melrose 1982; Robinson et al. 1994).

The probability for ion-scattering which appears in Equation (4) is

$$w_i^{LT}(\boldsymbol{k}_T, \boldsymbol{k}_L) = \frac{\sqrt{\pi}\omega_{\mathrm{pe}}^2}{2n_{\mathrm{e}}v_{T_{\mathrm{i}}}(1 + T_{\mathrm{e}}/T_{\mathrm{i}})^2} \frac{|\boldsymbol{k}_L \times \boldsymbol{k}_T|^2}{k_l^2 k_T^2 |\boldsymbol{k}_T - \boldsymbol{k}_L|} \exp\left(-\frac{(\omega_T - \omega_L)^2}{2|\boldsymbol{k}_T - \boldsymbol{k}_L|^2 v_{Ti}^2}\right), \quad (16)$$

identical to Equation (9). The main difference between this and the previous equation for Langmuir wave scattering is the cross product in the probability, which implies the emission peaks for scattering through $90°$.

For the three-wave scattering we have two alternatives

$$w^{LST}(\boldsymbol{k}, \boldsymbol{k}_L, \boldsymbol{k}_T) = \frac{\pi\omega_{\mathrm{pe}}^3 \left(1 + \frac{3T_i}{T_{\mathrm{e}}}\right)}{\omega_{k_T}^T 4n_{\mathrm{e}}T_{\mathrm{e}}} \omega_k^S \frac{|\boldsymbol{k}_T \times \boldsymbol{k}|^2}{k_T^2 |\boldsymbol{k}_L|^2} \delta(\omega_{k_T}^T - \omega_{k_L}^L \mp \omega_k^S), \quad (17)$$

where the minus sign in the delta function is used for the process $L+s \rightleftarrows t$, and the plus sign for $L \rightleftarrows t + s$. The only other difference between these two processes is a slight change in the participating wavenumbers, as we must consider $\boldsymbol{k}_t = \boldsymbol{k}_L \pm \boldsymbol{k}_s$ respectively. The three-wave probability also contains a cross product term, and is thus maximum for scattering by $90°$. In both cases (three-wave decay and ion-scattering), we have the condition $k_T \ll k_L$.

If we consider a realistic situation in the solar corona or wind, we have a beam of electrons with some small pitch angle spread. The Langmuir waves this produces also have a small angular spread, and this is only increased by the presence of plasma density fluctuations (e.g. Nishikawa & Riutov 1976), and by the ion-scattering and three-wave decays acting on the waves. The fundamental emission can therefore be rather non-directional when it is emitted. However, from the expression for the group velocity, Equation (15) and the dispersion relation, Equation (8), it is evident that emission close to the plasma frequency cannot propagate into plasma of increasing density. Ray tracing analyses by Li et al. (2006a) showed, using typical type III source parameters, that fundamental emission emitted into the forwards hemisphere at any angle is rapidly redirected to propagate along the direction of the magnetic field.

6 CONCLUSIONS

It is our opinion that solar radio physics is beginning to enter a new era. Regarding type IIIs, new technology is allowing simulations to generate synthetic dynamic spectra for comparison to observations to probe relevant electron beam and background plasma properties. At the same time, new technology is giving birth to the next generation of radio telescope. Interferometers with large baselines and huge collecting areas are being trained on the Sun to produce images of radio bursts over many frequencies with impressive angular resolution. We conclude this article by summarizing the future of type III radio burst analysis, both numerically and observationally.

6.1 "State of the Art" Simulations

While initially work on plasma emission was mainly theoretical, simulations have always played a key role. Early work by e.g. Takakura & Shibahashi (1976); Takakura (1982) allowed the simulation of bursts at a few wavelengths, and was key to the adoption of the ion-sound wave dependent model.

Only recently have large-scale kinetic simulations become possible, as computing power is a strong limitation. The series of papers by Li et al. (2008a,b, 2009) were the first to trace an electron beam from the injection site into the corona and solar wind, and calculate the resulting radio emission fully numerically, rather than by analytical estimates. These simulations have more recently been extended to cover a wider frequency range, and been used to explore the effects of the background plasma on the emission. In the solar wind, observations often show a kappa-distribution rather than a Maxwellian background plasma, and this contains more electrons with higher velocity. A similar power-law electron injection forms a higher velocity beam due to time-of-flight effects, and the emission may be expected to show a faster drift. This is confirmed by the simulations of Li & Cairns (2014), although they consider only instantaneous electron injection.

Ongoing work by the authors aims to combine the large-scale simulations of e.g. Reid & Kontar (2013) with a model for plasma radio emission used in a different context in Ratcliffe & Kontar (2014). This aims to explore the effects of plasma density fluctuations on the emission.

On the other hand, the fully numerical approach is not the only possibility. The simulations of Robinson & Cairns (1998); Cairns & Robinson (1999); Li et al. (2006b,a) used a combination of numerics and analytical estimates from SGT to reproduce emission. The relevance of SGT remains in question, but the results are useful nonetheless. The localization of Langmuir waves into discrete clumps, or wave packets, is investigated using the Zakharov equations in e.g. Zaslavsky et al. (2010); Krafft et al. (2013).

Continued work on the propagation of electrons and their Langmuir wave generation and non-linear evolution is also essential. Langmuir waves can help to explain the observed non-Maxwellian thermal electron distribution in the solar wind (e.g. Yoon et al. 2012b). They may affect the hard X-ray emission from downward electron beams in the corona (e.g. Hannah et al. 2013). Plasma emission has even been suggested as a source of sub-THz radio emission (Zaitsev et al. 2013).

6.2 Next Generation Radio Observations

There are many solar telescopes all around the world that are able to observe the dynamic spectra of type III radio bursts, too many to mention individually. On the global scale we would like to mention the e-Callisto project (Benz et al. 2009b), an international network of solar radio spectrometers that has more than 66 instruments in more than 35 locations with users from more than 92 countries.

Regarding imaging, the most notable dedicated solar interferometer for type III radio bursts is the NRH (Kerdraon & Delouis 1997), based in France, that has been making dedicated solar images since the 1960s, most recently between 150 MHz and 450 MHz.

The next generation radio observatories being developed around the world are taking observational solar radio astronomy into a revolutionary new phase. Large baseline interferometers are making high resolution imaging spectroscopy observations of type III bursts. This will enable us to address fundamental questions about the energy release site in solar flares and the transport of energetic electrons through the heliosphere. In Europe there is the LOw Frequency ARray (van Haarlem et al. 2013) (LOFAR), a network of observatories spread across Europe (Netherlands, UK, Germany, France and Sweden). LOFAR operates between the frequencies of 10 MHz and 250 MHz and is providing interferometric imaging with resolutions of 10s of arcsec. In North America there is the recently upgraded Expanded Very Large Array (Perley et al. 2011) (EVLA) that operates between 1 GHz and 50 GHz and has started solar observing at the end of 2011. In Western Australia there is the Murchison Widefield Array (MWA) (Lonsdale et al. 2009; Bowman et al. 2013) that is a low-frequency radio telescope operating between 80 MHz and 300 MHz, which is one of the precursors to the Square Kilometer Array (SKA) and has recently started to observe the Sun (Oberoi et al. 2011).

Other next generation radio telescopes are on the horizon and will soon be ready for solar observations. We now cover them (in no particular order). In China the Chinese Spectral Radio Heliograph (CSRH) (Yan et al. 2009) will be operational in 2014 and will produce dedicated solar imaging between 400 MHz and 15 GHz, an ideal frequency range for type III bursts in the deep corona. In Russia there is the Siberian Solar Radio Telescope (SSRT) that is being upgraded to create interferometric images of the Sun at GHz frequencies. In India an upgrade is currently under way to the Giant Metrewave Radio Telescope (GMRT) to operate between the frequencies of 50 MHz and 1500 MHz. In America, improvements to the existing array will create the Expanded Owens Valley Solar Array (EOVSA) that will operate between the frequency range 1 GHz to 18 GHz. In South America we will have the Brazilian Decimeric Array that will operate between the frequencies of 1 GHz and 6 GHz. In New Mexico there is the Long Wavelength Array (LWA) (Lazio et al. 2010; Taylor et al. 2012) that will operate at the low frequencies between $10 - 88$ MHz.

Extending into space, the upcoming ESA Solar Orbiter mission and NASA Solar Probe Plus mission are journeying close to the Sun to 10s of solar radii, and should both be launched in 2018. Both missions will be armed with in-situ plasma measuring devices to explore the radial dependence of type III radio signals and the plasma properties of electron beams and the ambient solar wind.

References

Abrami, A., Messerotti, M., Zlobec, P., & Karlicky, M. 1990, Sol. Phys., 130, 131

Alvarez, H., & Haddock, F. T. 1973a, Sol. Phys., 30, 175

Alvarez, H., & Haddock, F. T. 1973b, Sol. Phys., 29, 197

Arzner, K., & Benz, A. O. 2005, Sol. Phys., 231, 117

Arzner, K., & Magun, A. 1999, A&A, 351, 1165

Aschwanden, M. J., Benz, A. O., Dennis, B. R., & Schwartz, R. A. 1995a, ApJ, 455, 347

Aschwanden, M. J., Montello, M. L., Dennis, B. R., & Benz, A. O. 1995b, ApJ, 440, 394

Aschwanden, M. J., & Benz, A. O. 1997, ApJ, 480, 825

Aschwanden, M. J., Schwartz, R. A., & Dennis, B. R. 1998, ApJ, 502, 468

Aschwanden, M. J. 2012, A&A, 539, A2

Aurass, H., Klein, K.-L., & Martens, P. C. H. 1994, Sol. Phys., 155, 203

Aurass, H., & Klein, K.-L. 1997, A&AS, 123, 279

Bain, H. M., & Fletcher, L. 2009, A&A, 508, 1443

Bastian, T. S. 1994, ApJ, 426, 774

Benz, A. O., Barrow, C. H., Dennis, B. R., et al. 1983a, Sol. Phys., 83, 267

Benz, A. O., Bernold, T. E. X., & Dennis, B. R. 1983b, ApJ, 271, 355

Benz, A. O., Magun, A., Stehling, W., & Su, H. 1992, Sol. Phys., 141, 335

Benz, A. O., Grigis, P. C., Csillaghy, A., & Saint-Hilaire, P. 2005, Sol. Phys., 226, 121

Benz, A. O., Brajša, R., & Magdalenić, J. 2007, Sol. Phys., 240, 263

Benz, A. O., Monstein, C., Beverland, M., Meyer, H., & Stuber, B. 2009a, Sol. Phys., 260, 375

Benz, A. O., Monstein, C., Meyer, H., et al. 2009b, Earth Moon and Planets, 104, 277

Bonnin, X., Hoang, S., & Maksimovic, M. 2008, A&A, 489, 419

Bougeret, J.-L., Kaiser, M. L., Kellogg, P. J., et al. 1995, Space Sci. Rev., 71, 231

Bougeret, J. L., Goetz, K., Kaiser, M. L., et al. 2008, Space Sci. Rev., 136, 487

Bowman, J. D., Cairns, I., Kaplan, D. L., et al. 2013, PASA, 30, e031

Brazhenko, A. I., Melnik, V. N., Konovalenko, A. A., et al. 2012, Odessa Astronomical Publications, 25, 181

Bruno, R., & Carbone, V. 2005, Living Reviews in Solar Physics, 2, 4

Cairns, I. H., & Robinson, P. A. 1999, Physical Review Letters, 82, 3066

Cairns, I. H., Lobzin, V. V., Warmuth, A., et al. 2009, ApJ, 706, L265

Cane, H. V., Erickson, W. C., & Prestage, N. P. 2002, Journal of Geophysical Research (Space Physics), 107, 1315

Cane, H. V. 2003, ApJ, 598, 1403

Caroubalos, C., Poquerusse, M., & Steinberg, J. L. 1974, A&A, 32, 255

Celnikier, L. M., Harvey, C. C., Jegou, R., Moricet, P., & Kemp, M. 1983, A&A, 126, 293

Chen, B., Bastian, T. S., White, S. M., et al. 2013a, ApJ, 763, L21

Chen, C. H. K., Howes, G. G., Bonnell, J. W., et al. 2013b, in American Institute of Physics Conference Series, 1539, eds. G. P. Zank, J. Borovsky, R. Bruno, et al., 143

Chen, C. H. K., Salem, C. S., Bonnell, J. W., Mozer, F. S., & Bale, S. D. 2012, Physical Review Letters, 109, 035001

Chen, N., Ip, W.-H., & Innes, D. 2013c, ApJ, 769, 96

Cliver, E. W., & Ling, A. G. 2009, ApJ, 690, 598

Coles, W. A., & Harmon, J. K. 1989, ApJ, 337, 1023

Coles, W. A., Liu, W., Harmon, J. K., & Martin, C. L. 1991, J. Geophys. Res., 96, 1745

Crosby, N. B., Aschwanden, M. J., & Dennis, B. R. 1993, Sol. Phys., 143, 275

de La Noe, J., & Boischot, A. 1972, A&A, 20, 55

de La Noe, J. 1975, A&A, 43, 201

Dennis, B. R., Benz, A. O., Ranieri, M., & Simnett, G. M. 1984, Sol. Phys., 90, 383

Drummond, W. E., & Pines, D. 1962, Nucl. Fusion Suppl., 3, 1049

Dulk, G. A., & Suzuki, S. 1980, A&A, 88, 203

Dulk, G. A., Gary, D. E., & Suzuki, S. 1980, A&A, 88, 218

Dulk, G. A., Steinberg, J. L., & Hoang, S. 1984, A&A, 141, 30

Dulk, G. A. 1985, ARA&A, 23, 169

Dulk, G. A., Leblanc, Y., Robinson, P. A., Bougeret, J.-L., & Lin, R. P. 1998, J. Geophys. Res., 103, 17223

Dulk, G. A. 2000, Washington DC American Geophysical Union Geophysical Monograph Series, 119, 115

Dulk, G. A., Erickson, W. C., Manning, R., & Bougeret, J.-L. 2001, A&A, 365, 294

Eastwood, J. P., Wheatland, M. S., Hudson, H. S., et al. 2010, ApJ, 708, L95

Emslie, A. G., & Smith, D. F. 1984, ApJ, 279, 882

Emslie, A. G., Dennis, B. R., Shih, A. Y., et al. 2012, ApJ, 759, 71

Ergun, R. E., Larson, D., Lin, R. P., et al. 1998, ApJ, 503, 435

Ergun, R. E., Malaspina, D. M., Cairns, I. H., et al. 2008, Physical Review Letters, 101, 051101

Evans, L. G., Fainberg, J., & Stone, R. G. 1973, Sol. Phys., 31, 501

Fainberg, J., & Stone, R. G. 1970a, Sol. Phys., 15, 222

Fainberg, J., & Stone, R. G. 1970b, Sol. Phys., 15, 433

Fainberg, J., & Stone, R. G. 1971, Sol. Phys., 17, 392

Ginzburg, V. L., & Zhelezniakov, V. V. 1958, Soviet Ast., 2, 653

Glesener, L., Krucker, S., & Lin, R. P. 2012, ApJ, 754, 9

Goldman, M. V., & Dubois, D. F. 1982, Physics of Fluids, 25, 1062

Goldman, M. V. 1983, Sol. Phys., 89, 403

Gopalswamy, N. 2004, Planet. Space Sci., 52, 1399

Gopalswamy, N., & Mäkelä, P. 2010, ApJ, 721, L62

Gosling, J. T., Skoug, R. M., & McComas, D. J. 2003, Geophys. Res. Lett., 30, 130000

Graham, D. B., Cairns, I. H., Malaspina, D. M., & Ergun, R. E. 2012a, ApJ, 753, L18

Graham, D. B., Cairns, I. H., Prabhakar, D. R., et al. 2012b, J. Geophys. Res., (Space Physics), 117, A09107

Graham, D. B., & Cairns, I. H. 2013, Physical Review Letters, 111, 121101

Grognard, R. J.-M. 1985, Propagation of electron streams, 253 (Solar Radiophysics: Studies of Emission from the Sun at Metre Wavelengths)

Gurnett, D. A., & Anderson, R. R. 1976, Science, 194, 1159

Gurnett, D. A., & Anderson, R. R. 1977, J. Geophys. Res., 82, 632

Gurnett, D. A., Marsch, E., Pilipp, W., Schwenn, R., & Rosenbauer, H. 1979, J. Geophys. Res., 84, 2029

Haggerty, D. K., & Roelof, E. C. 2002, ApJ, 579, 841

Hamilton, R. J., & Petrosian, V. 1987, ApJ, 321, 721

Hamilton, R. J., Petrosian, V., & Benz, A. O. 1990, ApJ, 358, 644

Hannah, I. G., Christe, S., Krucker, S., et al. 2008, ApJ, 677, 704

Hannah, I. G., Kontar, E. P., & Sirenko, O. K. 2009, ApJ, 707, L45

Hannah, I. G., & Kontar, E. P. 2011, A&A, 529, A109

Hannah, I. G., Kontar, E. P., & Reid, H. A. S. 2013, A&A, 550, A51

Hoang, S., Poquerusse, M., & Bougeret, J.-L. 1997, Sol. Phys., 172, 307

Holman, G. D., Aschwanden, M. J., Aurass, H., et al. 2011, Space Sci. Rev., 159, 107

Huang, G. 1998, ApJ, 498, 877

Innes, D. E., Cameron, R. H., & Solanki, S. K. 2011, A&A, 531, L13

Isliker, H., & Benz, A. O. 1994, A&AS, 104, 145

Itkina, M. A., & Levin, B. N. 1992, A&A, 253, 521

Kahler, S. W., Krucker, S., & Szabo, A. 2011, J. Geophys. Res., (Space Physics), 116, A01104

Kai, K., Melrose, D. B., & Suzuki, S. 1985, Storms, 415

Kane, S. R. 1972, Sol. Phys., 27, 174

Kane, S. R. 1981, ApJ, 247, 1113

Kane, S. R., Benz, A. O., & Treumann, R. A. 1982, ApJ, 263, 423

Karlicky, M., Mann, G., & Aurass, H. 1996, A&A, 314, 303

Karlicky, M. 1998, Sol. Phys., 179, 421

Kayser, S. E., Bougeret, J.-L., Fainberg, J., & Stone, R. G. 1987, Sol. Phys., 109, 107

Kellogg, P. J., & Horbury, T. S. 2005, Annales Geophysicae, 23, 3765

Kellogg, P. J., Goetz, K., Monson, S. J., et al. 2009, J. Geophys. Res., (Space Physics), 114, A02107

Kerdraon, A., & Delouis, J.-M. 1997, in Coronal Physics from Radio and Space Observations (Lecture Notes in Physics, Berlin Springer Verlag), 483, ed. G. Trottet, 192

Klassen, A., Karlický, M., & Mann, G. 2003, A&A, 410, 307

Klassen, A., Gómez-Herrero, R., & Heber, B. 2011, Sol. Phys., 273, 413

Klassen, A., Gómez-Herrero, R., Heber, B., et al. 2012, A&A, 542, A28

Klein, K.-L., & Aurass, H. 1993, Advances in Space Research, 13, 295

Kontar', E. P., Lapshin, V. I., & Mel'Nik, V. N. 1998, Plasma Physics Reports, 24, 772

Kontar, E. P. 2001a, Sol. Phys., 202, 131

Kontar, E. P. 2001b, A&A, 375, 629

Kontar, E. P. 2001c, Plasma Physics and Controlled Fusion, 43, 589

Kontar, E. P., & Reid, H. A. S. 2009, ApJ, 695, L140

Kontar, E. P., & Jeffrey, N. L. S. 2010, A&A, 513, L2

Kontar, E. P., Brown, J. C., Emslie, A. G., et al. 2011, Space Sci. Rev., 159, 301

Kontar, E. P., Ratcliffe, H., & Bian, N. H. 2012, A&A, 539, A43

Krafft, C., Volokitin, A. S., & Krasnoselskikh, V. V. 2013, ApJ, 778, 111

Krucker, S., Larson, D. E., Lin, R. P., & Thompson, B. J. 1999, ApJ, 519, 864

Krucker, S., Kontar, E. P., Christe, S., & Lin, R. P. 2007, ApJ, 663, L109

Krucker, S., Oakley, P. H., & Lin, R. P. 2009, ApJ, 691, 806

Krucker, S., Kontar, E. P., Christe, S., Glesener, L., & Lin, R. P. 2011, ApJ, 742, 82

Kundu, M. R., Strong, K. T., Pick, M., et al. 1994, ApJ, 427, L59

Kundu, M. R., Raulin, J. P., Nitta, N., et al. 1995, ApJ, 447, L135

Labrum, N. R., & Stewart, R. T. 1970, Proceedings of the Astronomical Society of Australia, 1, 316

Lazio, T. J. W., Clarke, T. E., Lane, W. M., et al. 2010, AJ, 140, 1995

Le Chat, G., Issautier, K., Meyer-Vernet, N., et al. 2010, Twelfth International Solar Wind Conference, 1216, 316

Leblanc, Y., Dulk, G. A., & Hoang, S. 1995, Geophys. Res. Lett., 22, 3429

Leblanc, Y., Dulk, G. A., Hoang, S., Bougeret, J.-L., & Robinson, P. A. 1996, A&A, 316, 406

Lecacheux, A. 2000, Washington DC American Geophysical Union Geophysical Monograph Series, 119, 321

Ledenev, V. G., Zverev, E. A., & Starygin, A. P. 2004, Sol. Phys., 222, 299

Li, B., Robinson, P. A., & Cairns, I. H. 2006a, Physics of Plasmas, 13, 092902

Li, B., Robinson, P. A., & Cairns, I. H. 2006b, Physics of Plasmas, 13, 082305

Li, B., Cairns, I. H., & Robinson, P. A. 2008a, J. Geophys. Res., (Space Physics), 113, A06104

Li, B., Cairns, I. H., & Robinson, P. A. 2008b, J. Geophys. Res., (Space Physics), 113, A06105

Li, B., Cairns, I. H., & Robinson, P. A. 2009, J. Geophys. Res., (Space Physics), 114, A02104

Li, B., Cairns, I. H., & Robinson, P. A. 2011a, ApJ, 730, 21

Li, B., Cairns, I. H., & Robinson, P. A. 2011b, ApJ, 730, 20

Li, B., Cairns, I. H., Yan, Y. H., & Robinson, P. A. 2011c, ApJ, 738, L9

Li, B., Cairns, I. H., & Robinson, P. A. 2012, Sol. Phys., 279, 173

Li, B., & Cairns, I. H. 2014, Sol. Phys., 289, 951

Lin, R. P., Anderson, K. A., & Cline, T. L. 1972, Physical Review Letters, 29, 1035

Lin, R. P., Evans, L. G., & Fainberg, J. 1973, Astrophys. Lett., 14, 191

Lin, R. P., Potter, D. W., Gurnett, D. A., & Scarf, F. L. 1981, ApJ, 251, 364

Lin, R. P. 1985, Sol. Phys., 100, 537

Lin, R. P., Levedahl, W. K., Lotko, W., Gurnett, D. A., & Scarf, F. L. 1986, ApJ, 308, 954

Lin, R. P. 1990, in IAU Symposium 142, Basic Plasma Processes on the Sun, eds. E. R. Priest, & V. Krishan, 467

Lin, R. P., Anderson, K. A., Ashford, S., et al. 1995, Space Sci. Rev., 71, 125

Lin, R. P., Larson, D., McFadden, J., et al. 1996, Geophys. Res. Lett., 23, 1211

Lin, R. P., Dennis, B. R., Hurford, G. J., et al. 2002, Sol. Phys., 210, 3

Lonsdale, C. J., Cappallo, R. J., Morales, M. F., et al. 2009, IEEE Proceedings, 97, 1497

Lu, E. T., & Hamilton, R. J. 1991, ApJ, 380, L89

Ma, Y., Xie, R.-X., Zheng, X.-M., Wang, M., & Yan, Y. H. 2012, Chinese Astron. Astrophys., 36, 175

MacDowall, R. J., Lara, A., Manoharan, P. K., et al. 2003, Geophys. Res. Lett., 30, 8018

MacDowall, R. J., Richardson, I. G., Hess, R. A., & Thejappa, G. 2009, in IAU Symposium, 257, eds. N. Gopalswamy, & D. F. Webb, 335

Magelssen, G. R., & Smith, D. F. 1977, Sol. Phys., 55, 211

Maksimovic, M., Zouganelis, I., Chaufray, J.-Y., et al. 2005, J. Geophys. Res., (Space Physics), 110, A09104

Marsch, E., & Tu, C.-Y. 1990, J. Geophys. Res., 95, 11945

Maxwell, A., & Swarup, G. 1958, Nature, 181, 36

McClements, K. G. 1987a, A&A, 175, 255

McClements, K. G. 1987b, Sol. Phys., 109, 355

McLean, D. J. 1971, Australian Journal of Physics, 24, 201

Meléndez, J. L., Sawant, H. S., Fernandes, F. C. R., & Benz, A. O. 1999, Sol. Phys., 187, 77

Mel'Nik, V. N. 1995, Plasma Physics Reports, 21, 89

Mel'Nik, V. N., Lapshin, V., & Kontar, E. 1999, Sol. Phys., 184, 353

Mel'Nik, V. N., & Kontar, E. P. 2003, Sol. Phys., 215, 335

Mel'Nik, V. N., Konovalenko, A. A., Abranin, E. P., et al. 2005, Astronomical and Astrophysical Transactions, 24, 391

Melnik, V. N., Konovalenko, A. A., Rucker, H. O., & Lecacheux, A. 2007, Highlights of Astronomy, 14, 365

Melnik, V. N., Rucker, H. O., Konovalenko, A. A., et al. 2010, in American Institute of Physics Conference Series, 1206, eds. S. K. Chakrabarti, A. I. Zhuk, & G. S. Bisnovatyi-Kogan, 445

Melnik, V. N., Konovalenko, A. A., Rucker, H. O., et al. 2011, Sol. Phys., 269, 335

Melrose, D. B., & Sy, W. N. 1972, Australian Journal of Physics, 25, 387

Melrose, D. B., Dulk, G. A., & Smerd, S. F. 1978, A&A, 66, 315

Melrose, D. B., & Stenhouse, J. E. 1979, A&A, 73, 151

Melrose, D. B. 1980a, Plasma Astrophysics: Nonthermal Processes in Diffuse Magnetized Plasmas - Vol.2 - Astrophysical Applications, 430 (New York: Gordon and Breach Science Publishers)

Melrose, D. B. 1980b, Plasma Astrohysics. Nonthermal Processes in Diffuse Magnetized Plasmas - Vol.1 - The Emission, Absorption and Transfer of Waves in Plasmas

Melrose, D. B. 1980c, Space Sci. Rev., 26, 3

Melrose, D. B., Dulk, G. A., & Gary, D. E. 1980, Proceedings of the Astronomical Society of Australia, 4, 50

Melrose, D. B. 1982, Sol. Phys., 79, 173

Melrose, D. B. 1983, Sol. Phys., 87, 359

Melrose, D. B. 1987, Sol. Phys., 111, 89

Melrose, D. B. 1989a, Sol. Phys., 119, 143

Melrose, D. B. 1989b, Sol. Phys., 120, 369

Melrose, D. B. 2009, in IAU Symposium, 257, eds. N. Gopalswamy, & D. F. Webb, 305

Mercier, C. 1990, Sol. Phys., 130, 119

Mercier, C., & Trottet, G. 1997, ApJ, 474, L65

Morioka, A., Miyoshi, Y., Masuda, S., et al. 2007, ApJ, 657, 567

Muschietti, L., Goldman, M. V., & Newman, D. 1985, Sol. Phys., 96, 181

Newbury, J. A., Russell, C. T., Phillips, J. L., & Gary, S. P. 1998, J. Geophys. Res., 103, 9553

Nishikawa, K., & Riutov, D. D. 1976, Journal of the Physical Society of Japan, 41, 1757

Nita, G. M., Gary, D. E., Lanzerotti, L. J., & Thomson, D. J. 2002, ApJ, 570, 423

Nitta, N. V., Mason, G. M., Wiedenbeck, M. E., et al. 2008, ApJ, 675, L125

Oberoi, D., Matthews, L. D., Cairns, I. H., et al. 2011, ApJ, 728, L27

Pavan, J., Ziebell, L. F., Gaelzer, R., & Yoon, P. H. 2009a, J. Geophys. Res., (Space Physics), 114, A01106

Pavan, J., Ziebell, L. F., Yoon, P. H., & Gaelzer, R. 2009b, Plasma Physics and Controlled Fusion, 51, 095011

Pearson, K. 1895, Royal Society of London Philosophical Transactions Series A, 186, 343

Perley, R. A., Chandler, C. J., Butler, B. J., & Wrobel, J. M. 2011, ApJ, 739, L1

Pick, M., Mason, G. M., Wang, Y.-M., Tan, C., & Wang, L. 2006, ApJ, 648, 1247

Pick, M., & Vilmer, N. 2008, A&A Rev., 16, 1

Poquerusse, M. 1994, A&A, 286, 611

Ratcliffe, H., Bian, N. H., & Kontar, E. P. 2012, ApJ, 761, 176

Ratcliffe, H., & Kontar, E. P. 2014, A&A, 562, A57

Raulin, J. P., Kundu, M. R., Hudson, H. S., Nitta, N., & Raoult, A. 1996, A&A, 306, 299

Reid, H. A. S., & Kontar, E. P. 2010, ApJ, 721, 864

Reid, H. A. S., Vilmer, N., & Kontar, E. P. 2011, A&A, 529, A66

Reid, H. A. S., & Kontar, E. P. 2013, Sol. Phys., 285, 217

Reid, H. A. S., Vilmer, N., & Kontar, E. P. 2014, arXiv: 1403.1839

Reiner, M. J., Fainberg, J., Kaiser, M. L., & Bougeret, J.-L. 2007, Sol. Phys., 241, 351

Rha, K., Ryu, C.-M., & Yoon, P. H. 2013, ApJ, 775, L21

Riddle, A. C. 1972, Proceedings of the Astronomical Society of Australia, 2, 98

Robinson, R. D. 1977, Sol. Phys., 55, 459

Robinson, P. A. 1992, Sol. Phys., 139, 147

Robinson, P. A., Cairns, I. H., & Gurnett, D. A. 1992, ApJ, 387, L101

Robinson, P. A., Cairns, I. H., & Willes, A. J. 1994, ApJ, 422, 870

Robinson, P. A., & Cairns, I. H. 1994, Sol. Phys., 154, 335

Robinson, P. A., & Cairns, I. H. 1998, Sol. Phys., 181, 363

Robinson, P. A., & Benz, A. O. 2000, Sol. Phys., 194, 345

Ryutov, D. D. 1969, Soviet Journal of Experimental and Theoretical Physics, 30, 131

Saint-Hilaire, P., Krucker, S., Christe, S., & Lin, R. P. 2009, ApJ, 696, 941

Saint-Hilaire, P., Vilmer, N., & Kerdraon, A. 2013, ApJ, 762, 60

Sirenko, O., Voitenko, Y., & Goossens, M. 2002, A&A, 390, 725

Smith, D. F. 1970, Sol. Phys., 15, 202

Smith, D. F., & Riddle, A. C. 1975, Sol. Phys., 44, 471

Smith, R. A., Goldstein, M. L., & Papadopoulos, K. 1976, Sol. Phys., 46, 515

Smith, D. F., & Sime, D. 1979, ApJ, 233, 998

Spangler, S. R. 2002, ApJ, 576, 997

Staehli, M., & Benz, A. O. 1987, A&A, 175, 271

Steinberg, J. L., Aubier-Giraud, M., Leblanc, Y., & Boischot, A. 1971, A&A, 10, 362

Steinberg, J.-L. 1972, A&A, 18, 382

Steinberg, J. L., Hoang, S., & Dulk, G. A. 1985, A&A, 150, 205

Stewart, R. T. 1974, Sol. Phys., 39, 451

Sturrock, P. A. 1964, NASA Special Publication, 50, 357

Suzuki, S., & Sheridan, K. V. 1977, Izvestiia Vysshaia Uchebn. Zaved., Radiofizika, 20, 1432

Suzuki, S., & Sheridan, K. V. 1978, Radiophysics and Quantum Electronics, 20, 989

Suzuki, S., & Dulk, G. A. 1985, Bursts of Type III and Type V (Solar Radiophysics: Studies of Emission from the Sun at Metre Wavelengths), 289

Takakura, T., & Shibahashi, H. 1976, Sol. Phys., 46, 323

Takakura, T. 1982, Sol. Phys., 78, 141

Tan, L. C., Reames, D. V., Ng, C. K., Shao, X., & Wang, L. 2011, ApJ, 728, 133

Tang, J. F., Wu, D. J., & Tan, C. M. 2013, ApJ, 779, 83

Taylor, G. B., Ellingson, S. W., Kassim, N. E., et al. 2012, Journal of Astronomical Instrumentation, 1, 1250004

Thejappa, G., Lengyel-Frey, D., Stone, R. G., & Goldstein, M. L. 1993, ApJ, 416, 831

Thejappa, G., MacDowall, R. J., Bergamo, M., & Papadopoulos, K. 2012, ApJ, 747, L1

Thejappa, G., MacDowall, R. J., & Bergamo, M. 2013, J. Geophys. Res., (Space Physics), 118, 4039

Tsytovich, V. N. 1995, Lectures on Non-linear Plasma Kinetics, XI (Springer-Verlag Berlin Heidelberg New York. Also Springer Series on Atoms and Plasmas, volume 17)

van Allen, J. A., & Krimigis, S. M. 1965, J. Geophys. Res., 70, 5737

van Haarlem, M. P., Wise, M. W., Gunst, A. W., et al. 2013, A&A, 556, A2

Vedenov, A. A., Velikhov, E. P., & Sagdeev, R. Z. 1962, Nucl. Fusion Suppl., 2, 465

Vedenov, A. A., Gordeev, A. V., & Rudakov, L. I. 1967, Plasma Physics, 9, 719

Vedenov, A. A., & Ryutov, D. D. 1972, Voprosu Teorii Plasmu, 6, 3

Vidojević, S., Zaslavsky, A., Maksimović, M., Dražić, M., & Atanacković, O. 2011, Baltic Astronomy, 20, 596

Vidojevic, S., Zaslavsky, A., Maksimovic, M., et al. 2012, Publications of the Astronomical Society "Rudjer Boskovic", 11, 343

Voshchepynets, A., & Krasnoselskikh, V. 2013, Annales Geophysicae, 31, 1379

Wang, J. R., Fisk, L. A., & Lin, R. P. 1971, International Cosmic Ray Conference, 2, 438

Wang, M., Duan, C. C., Xie, R. X., & Yan, Y. H. 2003, Sol. Phys., 212, 401

Wang, L., Lin, R. P., Krucker, S., & Gosling, J. T. 2006, Geophys. Res. Lett., 33, L03106

Wang, L., Lin, R. P., & Krucker, S. 2011, ApJ, 727, 121

Wang, L., Lin, R. P., Krucker, S., & Mason, G. M. 2012, ApJ, 759, 69

Weber, R. R. 1978, Sol. Phys., 59, 377

Weiss, L. A. A., & Stewart, R. T. 1965, Australian Journal of Physics, 18, 143

Wentzel, D. G. 1984, Sol. Phys., 90, 139

Wild, J. P., & McCready, L. L. 1950, Australian Journal of Scientific Research A Physical Sciences, 3, 387

Wild, J. P., Murray, J. D., & Rowe, W. C. 1954, Australian Journal of Physics, 7, 439

Wild, J. P., Sheridan, K. V., & Trent, G. H. 1959, in IAU Symposium, 9, URSI Symp. 1: Paris Symposium on Radio Astronomy, ed. R. N. Bracewell, 176

Willes, A. J., Robinson, P. A., & Melrose, D. B. 1996, Physics of Plasmas, 3, 149

Willes, A. J., & Melrose, D. B. 1997, Sol. Phys., 171, 393

Winglee, R. M., & Dulk, G. A. 1986, ApJ, 310, 432

Woo, R., Armstrong, J. W., Bird, M. K., & Patzold, M. 1995, Geophys. Res. Lett., 22, 329

Wu, C. S., Wang, C. B., Yoon, P. H., Zheng, H. N., & Wang, S. 2002, ApJ, 575, 1094

Yan, Y., Zhang, J., Wang, W., et al. 2009, Earth Moon and Planets, 104, 97

Yoon, P. H., Rhee, T., & Ryu, C.-M. 2005, Physical Review Letters, 95, 215003

Yoon, P. H., Hong, J., Kim, S., et al. 2012a, ApJ, 755, 112

Yoon, P. H., Ziebell, L. F., Gaelzer, R., Lin, R. P., & Wang, L. 2012b, Space Sci. Rev., 173, 459

Zaitsev, V. V., Mityakov, N. A., & Rapoport, V. O. 1972, Sol. Phys., 24, 444

Zaitsev, V. V., Stepanov, A. V., & Melnikov, V. F. 2013, Astronomy Letters, 39, 650

Zakharov, V. E. 1972, Soviet Journal of Experimental and Theoretical Physics, 35, 908

Zaslavsky, A., Volokitin, A. S., Krasnoselskikh, V. V., Maksimovic, M., & Bale, S. D. 2010, J. Geophys. Res., (Space Physics), 115, A08103

Zharkova, V. V., & Siversky, T. V. 2011, ApJ, 733, 33

Zheleznyakov, V. V., & Zlotnik, E. Y. 1964, Soviet Ast., 7, 485

Zheleznyakov, V. V., & Zaitsev, V. V. 1970, Soviet Ast., 14, 47

Zheleznyakov, V. V., & Zlotnik, E. Y. 1974, Sol. Phys., 36, 443

Ziebell, L. F., Gaelzer, R., Pavan, J., & Yoon, P. H. 2008a, Plasma Physics and Controlled Fusion, 50, 085011

Ziebell, L. F., Gaelzer, R., & Yoon, P. H. 2008b, Physics of Plasmas, 15, 032303

Ziebell, L. F., Yoon, P. H., Pavan, J., & Gaelzer, R. 2011, ApJ, 727, 16

Ziebell, L. F., Yoon, P. H., Gaelzer, R., & Pavan, J. 2012, Plasma Physics and Controlled Fusion, 54, 055012